

High-order thermal lattice Boltzmann models derived by means of Gauss quadrature in the spherical coordinate system

Victor Eugen Ambrus*

Department of Physics, West University of Timișoara, Boulevard Vasile Pârvan 4, Timișoara R-300223, Romania

Victor Sofonea†

Center for Fundamental and Advanced Technical Research, Romanian Academy, Boulevard Mihai Viteazul 24, Timișoara R-300223, Romania

(Received 14 April 2012; published 20 July 2012)

We use the spherical coordinate system in the momentum space and an appropriate discretization procedure to derive a hierarchy of lattice Boltzmann (LB) models with variable temperature. The separation of the integrals in the momentum space into angular and radial parts allows us to compute the moments of the equilibrium distribution function by means of Gauss-Legendre and Gauss-Laguerre quadratures, as well as to find the elements of the discrete momentum set for each LB model in the hierarchy. The capability of the high-order models in this hierarchy to capture specific effects in microfluidics is investigated through a computer simulation of Couette flow by using the Shakhov collision term to get the right value of the Prandtl number.

DOI: [10.1103/PhysRevE.86.016708](https://doi.org/10.1103/PhysRevE.86.016708)

PACS number(s): 47.11.-j, 47.61.-k, 51.10.+y

I. INTRODUCTION

Lattice Boltzmann (LB) models are derived from the Boltzmann equation using a simplified version of the collision operator, as well as an appropriate discretization of the phase space [1–4]. Since discrete velocity sets $\{\mathbf{v}_i, i = 1, 2, \dots, \mathcal{N}\}$ provide a basic ingredient of LB models, these models are a particular class of discrete velocity models (DVM) introduced five decades ago in the kinetic theory of rarefied gases to approximate the collision operator [5–8]. LB models originated more than 20 years ago [9–12] from the lattice gas automata [3, 13–15] and were primarily designed to recover the hydrodynamics of fluid systems at the Navier-Stokes level by using a *polynomial expansion* of the equilibrium distribution function. In their early days, the LB models inherited the *collision-streaming* concept, the main characteristics of their ancestors. According to this concept, all fluid particles that collided in a node \mathbf{r} of the lattice move thereafter (in a lapse δt) along the lattice links towards \mathcal{N} neighboring nodes whose position vectors are \mathbf{r}_i . To achieve this feature, the discrete velocities \mathbf{v}_i are related to the lattice geometry and satisfy the relation

$$|\mathbf{v}_i| \delta t = |\mathbf{r}_i - \mathbf{r}|, \quad i = 1, 2, \dots, \mathcal{N}. \quad (1)$$

Such discrete velocity sets, called *space filling* velocity sets, are very difficult to build for thermal LB models, especially when higher-order moments of the equilibrium distribution function need to be achieved [16–27]. *Off-lattice* velocity sets that do not satisfy Eq. (1) were later considered in LB models by using finite-difference, finite-volume, or flux limiter schemes [28–44]. LB models provide an alternative to the simulation techniques of computational fluid dynamics (CFD) or direct simulation Monte Carlo (DSMC) and have been recognized as efficient tools for the investigation of single-component or multicomponent complex fluids with or without structure

formation [1–4, 45–60], as well as for the investigation of microfluidics problems [17, 28–30, 61–77].

In microscale and nanoscale flows, the nonequilibrium behavior of the fluid on length scales of the order of the mean free path λ of fluid particles produces a wealth of effects not properly captured by standard hydrodynamics based on the Navier-Stokes-Fourier equations [78–88]. Such effects are observed when the Knudsen number $\text{Kn} = \lambda/L$, defined as the ratio between λ and the characteristic size L of the flow domain, becomes noticeable ($\text{Kn} > 0.001$). In particular, the velocity slip, the temperature jump, as well as the longitudinal heat flux that is not driven by the temperature gradient are specific effects that manifest themselves at the microscale in the case of Couette flow between parallel plates moving in opposite directions [17, 29, 62–74, 76–88].

As pointed by Karlin and coworkers [17, 66–68, 74], as well as by other authors [18–24, 69–73, 76, 77, 89–93], successive members of a hierarchy of LB models are needed to account for the complexity of flow phenomena in a fluid system as the Knudsen number increases and the system goes farther away from equilibrium. The LB models of the hierarchy and the corresponding discrete velocity sets are usually derived by means of the Gauss-Hermite quadrature in the momentum space after the separation of variables in the Cartesian coordinate system [17–24, 66–68, 74, 89–95]. Higher-order moments of the equilibrium distribution function are successively satisfied when increasing the position of an LB model in the hierarchy. Unfortunately, most of the models derived using this strategy and currently reported in the literature are mainly isothermal or of low order. Moreover, the widely used two-dimensional LB models do not account for the real number of degrees of freedom in the physical space and might not be appropriate for investigating energy transport phenomena. Although much effort was devoted recently to develop accurate LB models with variable temperature [17–24, 66–68, 74, 89–93], such high-order models are still needed for the investigation of flow phenomena in microfluidics.

In their pioneering works [31–33], Watari and Tsutahara introduced two-dimensional (2D), as well as three-dimensional

*victor.ambrus@gmail.com

†Corresponding author: sofonea@acad-tim.tm.edu.ro

(3D) LB models with variable temperature, where moments of the distributions function are fulfilled up to fourth order. A characteristic of these models is that the discrete velocities lie on circular (2D) or spherical (3D) shells, respectively. Inspired by the spherical shell concept, in this paper we introduce a general procedure to derive LB models of arbitrary order N in the space with $D = 3$ dimensions by using the spherical coordinate system in the momentum space, as well as Gauss quadrature.

The paper is organized as follows. In Sec. II we discuss the discretization procedure of the momentum space by using the separation of variables in the spherical coordinate system followed by appropriate Gauss quadrature. The resulting *spherical shell* LB models (SLB) are summarized in Sec. III. Since the single relaxation time (Bhatnagar-Gross-Krook, BGK) collision term [1–4] does not ensure the right value of the Prandtl number for the ideal gas in the LB models, we use the Shakhov collision term [96–99] instead. The Shakhov collision term and the conservation equations are discussed in Sec. IV. The numerical scheme we use to solve the evolution equations of the distribution functions, as well as the implementation of boundary conditions, are discussed in Sec. V. Computer simulation results for Couette flow at various values of the Knudsen number are reported in Secs. VI and VII, the first of which is focused on the investigation of the accuracy of the SLB models, while the second one is committed to optimal models for fluid flow at the Navier-Stokes-Fourier level ($\text{Kn} \leq 0.1$). Section VIII summarizes our results and concludes the paper.

Details related to Gauss quadrature, as well as to the Legendre and generalized Laguerre polynomials used to build the discrete velocity sets and the corresponding equilibrium distribution functions in the SLB models are provided in the Appendixes. There is also a short appendix dedicated to Hermite polynomials, which are used in Sec. IV.

Throughout this paper we use dimensionless quantities that are derived by means of three basic reference quantities [100]: a characteristic length l_R , a reference mass m_R , and a reference energy $e_R = k_B T_R$ (k_B is Boltzmann's constant and T_R is a reference temperature). Other quantities of interest are made dimensionless using the references that are derived from the basic quantities: particle number density $n_R = 1/l_R^D$, speed $c_R = \sqrt{k_B T_R/m_R}$, time l_R/c_R , and so on. Note that, although we deal with a single component fluid system in this paper, we do not necessarily choose m_R equal to the mass of fluid particles. This allows us to keep the dimensionless value $m \neq 1$ of the mass of fluid particles in the equations to follow and to facilitate their readability, as well as their extension to multicomponent fluid systems in future publications.

II. DISCRETIZATION OF THE MOMENTUM SPACE

A. Separation of variables in the spherical coordinate system

To ensure the isotropy, we take advantage of the *spherical shell* models introduced by Watari and Tsutahara [31–33, 101–103] and build a hierarchy of thermal LB models in the 3D space by using the spherical coordinate system in the momentum space instead of the Cartesian one that is currently used in LB models derived by Gauss-Hermite quadrature

[18,28–30]. The discretization procedure of the momentum space is the keystone of any LB model and should fulfill the fundamental conditions outlined by Chen and Shan [91]. Following this procedure, the continuum momentum space is replaced by a discrete set $\{\mathbf{p}_{kji}\}$. The corresponding density functions and equilibrium density functions are denoted f_{kji} and $f_{kji}^{(eq)}$, respectively (the meaning of the integer indices k, j, i , as well as their range, will arise later).

The highest natural number N for which all tensors of order s ($0 \leq s \leq N$)

$$\widetilde{\mathcal{M}}_{\{\alpha_i\}}^{(s)} \equiv \widetilde{\mathcal{M}}_{\alpha_1, \alpha_2, \dots, \alpha_s}^{(s)} = \sum_{k, j, i} f_{kji}^{(eq)} \prod_{l=1}^s p_{kji\alpha_l} \quad (2)$$

equal the corresponding ones in the continuum space [91]

$$\mathcal{M}_{\{\alpha_i\}}^{(s)} \equiv \mathcal{M}_{\alpha_1, \alpha_2, \dots, \alpha_s}^{(s)} = \int d^D p f^{(eq)} \prod_{l=1}^s p_{\alpha_l} \quad (3)$$

defines the order of the LB model in the hierarchy ($p_{kji\alpha_l}$ and p_{α_l} , $\alpha_l \in \{1, 2, 3\}$ are the Cartesian components of the vectors \mathbf{p}_{kji} and \mathbf{p} , respectively). For a given N , the moments \mathbf{p}_{kji} , as well as the corresponding equilibrium density functions $f_{kji}^{(eq)}$ will be established in Sec. II B by means of series expansion and Gauss quadrature.

We first note that the equilibrium distribution function in the continuum space, i.e. the Maxwell - Boltzmann distribution function, is given by

$$f^{(eq)} \equiv f^{(eq)}(\mathbf{p}; n, \mathbf{u}, T) = n(\beta/\pi)^{D/2} e^{-\beta(\mathbf{p}-m\mathbf{u})^2}, \quad (4)$$

where the particle number density n , fluid velocity u_α , and fluid temperature T [1–4] are given by ($\beta = 1/2mT$, $\delta_{\alpha_1\alpha_2}$ is Kronecker's symbol and the sum rule over repeated α_i indices is understood)

$$n = \mathcal{M}^{(0)}, \quad (5a)$$

$$u_\alpha = \mathcal{M}_\alpha^{(1)}/mn, \quad (5b)$$

$$T = \delta_{\alpha_1\alpha_2} \mathcal{M}_{\alpha_1\alpha_2}^{(2)}/Dmn - mu^2/D. \quad (5c)$$

Since mass, momentum, and energy are conserved during fluid particle collisions, the local quantities n , u_α , and T are also recovered by computing the corresponding moments of f_{kji} and f [1–4, 18–20, 89–91]. Splitting Eq. (4) yields ($p \equiv \sqrt{\mathbf{p}^2}$)

$$f^{(eq)} \equiv f^{(eq)}(\mathbf{p}; n, \mathbf{u}, T) = nF(p^2; T)E(\mathbf{p}; \mathbf{u}, T), \quad (6a)$$

$$F \equiv F(p^2; T) = (\beta/\pi)^{D/2} e^{-\beta p^2}, \quad (6b)$$

$$E \equiv E(\mathbf{p}; \mathbf{u}, T) = e^{-\beta(m^2 u^2 - 2m \mathbf{p} \cdot \mathbf{u})}. \quad (6c)$$

Before expanding E in a power series with respect to $u/\sqrt{T/m}$ to get $\{\mathbf{p}_{kji}\}$ and $f_{kji}^{(eq)}$ that ensure

$$\widetilde{\mathcal{M}}_{\alpha_1, \alpha_2, \dots, \alpha_s}^{(s)} = \mathcal{M}_{\alpha_1, \alpha_2, \dots, \alpha_s}^{(s)} \quad (7)$$

for $0 \leq s \leq N$, we follow [91] and note that

$$p_\alpha E = (T \partial_{u_\alpha} + m u_\alpha) E, \quad (8)$$

$$f^{(eq)} \prod_{l=1}^s p_{\alpha_l} = n F \prod_{l=1}^s (T \partial_{u_{\alpha_l}} + m u_{\alpha_l}) E. \quad (9)$$

Since \mathbf{p} and \mathbf{u} are independent variables, the differential operator $T\partial_{u_\alpha} + mu_\alpha$ commutes with the integration operator. Thus the s th order tensor

$$\begin{aligned}\mathcal{M}_{\alpha_1, \alpha_2, \dots, \alpha_s}^{(s)} &= \int d^D p n F \prod_{l=1}^s (T\partial_{u_{\alpha_l}} + mu_{\alpha_l}) E \\ &= \left[\prod_{l=1}^s (T\partial_{u_{\alpha_l}} + mu_{\alpha_l}) \right] \int d^D p f^{(\text{eq})} \\ &= \left[\prod_{l=1}^s (T\partial_{u_{\alpha_l}} + mu_{\alpha_l}) \right] n\end{aligned}\quad (10)$$

is a polynomial of order s with respect to the Cartesian components of the fluid velocity \mathbf{u} [91]. Hence Eq. (3) is preserved for $0 \leq s \leq N$ when replacing E in Eq. (6a) with its series expansion up to order N with respect to \mathbf{u}

$$E^{(N)} = \sum_{j=0}^{\lfloor N/2 \rfloor} \frac{1}{j!} \left(-\frac{m\mathbf{u}^2}{2T} \right)^j \sum_{r=0}^{N-2j} \frac{1}{r!} \left(\frac{\mathbf{p} \cdot \mathbf{u}}{T} \right)^r \quad (11)$$

($\lfloor x \rfloor$ is the largest integer less than or equal to x). When using the spherical coordinates (p, θ, φ) to express the Cartesian projections p_α of the momentum vector \mathbf{p} , we get

$$p_\alpha = p_\alpha(p, \theta, \varphi) = p e_\alpha(\theta, \varphi), \quad \alpha \in \{1, 2, 3\}, \quad (12)$$

where

$$\begin{aligned}e_1(\theta, \varphi) &= \sin \theta \cos \varphi, e_2(\theta, \varphi) = \sin \theta \sin \varphi, \\ e_3(\theta, \varphi) &= \cos \theta.\end{aligned}\quad (13)$$

Hence

$$E^{(N)} \equiv E^{(N)}(p, \theta, \varphi; \mathbf{u}, T) \quad (14)$$

and

$$\mathcal{M}_{\{\alpha_i\}}^{(s)} = n \int_0^\infty dp p^{D-1} F \int_{-1}^{+1} d(\cos \theta) \int_0^{2\pi} d\varphi \mathcal{S}_{\{\alpha_i\}}^{(s)}(\theta, \varphi). \quad (15)$$

The term $\mathcal{S}_{\{\alpha_i\}}^{(s)}(\theta, \varphi)$ in the last integral above is a trigonometric polynomial of the form

$$\begin{aligned}\mathcal{S}_{\{\alpha_i\}}^{(s)}(\theta, \varphi) &= p^s E^{(N)} \prod_{l=1}^s e_{\alpha_l}(\theta, \varphi) \\ &= \sum_{s \leq \lambda + \mu + \nu \leq s + N} A_{\lambda, \mu, \nu}(p; \mathbf{u}, T) \\ &\quad \times (\cos \theta)^\lambda (\sin \theta)^{\mu + \nu} (\cos \varphi)^\mu (\sin \varphi)^\nu,\end{aligned}\quad (16)$$

where λ, μ, ν are positive integer numbers and the real coefficients $A_{\lambda, \mu, \nu}(p; \mathbf{u}, T)$ do not depend on θ and φ .

B. Gauss quadratures

Following the discretization procedure, the continuum momentum space is replaced by a discrete set $\{\mathbf{p}_{kji}\}$. The Cartesian components of the vectors \mathbf{p}_{kji} are $p_{kji\alpha} = p_k e_\alpha(\theta_j, \varphi_i)$. An LB model of order N is derived using a discretization procedure that ensures Eq. (7) (i.e., the *exact recovery* of all moments of the equilibrium distribution function up to order N).

This section presents a specific method used for the discretization of the momentum space. The method is designed to ensure the exact recovery of moments of the equilibrium distribution function by Gauss quadrature (some general information can be found in Appendix A). The choice of a discrete set of momenta is dictated by precise quadrature rules, which ensure the exact recovery of the angular and radial integrals in Eq. (15).

According to [104,105], the following quadrature formula is exact

$$\mathcal{Q}_{\{\alpha_i\}}^{(s)} = \int_0^{2\pi} d\varphi \mathcal{S}_{\{\alpha_i\}}^{(s)}(\theta, \varphi) = \frac{2\pi}{M} \sum_{i=1}^M \mathcal{S}_{\{\alpha_i\}}^{(s)}(\theta, \varphi_i) \quad (17)$$

provided that

$$\varphi_i = \phi + 2\pi \frac{i-1}{M}, \quad M \geq 2N + 1, \quad (18)$$

where ϕ is an arbitrary angle. Since $\sin(\varphi - \pi) = -\sin \varphi$ and $\cos(\varphi - \pi) = -\cos \varphi$, one has

$$\int_0^{2\pi} d\varphi (\cos \varphi)^\mu (\sin \varphi)^\nu = (-1)^{\mu+\nu} \int_0^{2\pi} d\varphi (\cos \varphi)^\mu (\sin \varphi)^\nu.$$

Consequently, terms with odd $(\mu + \nu)$ in $\mathcal{S}_{\{\alpha_i\}}^{(s)}(\theta, \varphi)$ do not contribute to the integral with respect to φ in Eq. (15).

The even powers of $\sin \theta$ in Eq. (16) are easily changed to powers of $\cos \theta$ and $\mathcal{Q}_{\{\alpha_i\}}^{(s)}$ is eventually expressed as a polynomial of order at most $2N$ in $z = \cos \theta$. The *Gauss-Legendre* quadrature [105–107] gives

$$\mathcal{E}_{\{\alpha_i\}}^{(s)} = \int_{-1}^{+1} dz \mathcal{Q}_{\{\alpha_i\}}^{(s)} = \sum_{j=1}^L w_j^{(P)} \mathcal{Q}_{\{\alpha_i\}}^{(s)}(z_j), \quad (19)$$

where z_j , $1 \leq j \leq L$ are the roots of the Legendre polynomial $P_L(z)$ of order $L \geq N + 1$ and

$$w_j^{(P)} = \frac{2(1 - z_j^2)}{(L+1)^2 [P_{L+1}(z_j)]^2} \quad (20)$$

are their associated weights. More insight on Legendre polynomials and the Gauss-Legendre quadrature method is provided in Appendix B.

The quadrature points

$$\theta_j \equiv \arccos(z_j), \quad (21a)$$

$$\varphi_i = \phi + 2\pi(i-1)/M \quad (21b)$$

that are used to retrieve the angular integrals in the *spherical shell* LB model define a discrete set e_{ji} ($1 \leq j \leq L$, $1 \leq i \leq M$) of vectors on the unit sphere, with the Cartesian projections

$$e_{ji\alpha} \equiv e_\alpha(\theta_j, \varphi_i), \quad \alpha \in \{1, 2, 3\} \quad (22)$$

given by Eq. (13).

Due to the symmetry of the integration domain, odd powers of $z = \cos \theta$ do not contribute to $\mathcal{E}_{\{\alpha_i\}}^{(s)}$. Thus the appropriate use of quadrature formulas during integration over the angular coordinates (θ, φ) gives the polynomial $\mathcal{E}_{\{\alpha_i\}}^{(s)} \equiv \mathcal{E}_{\{\alpha_i\}}^{(s)}(p^2; \mathbf{u}, T)$ containing only even powers of p

$$\mathcal{E}_{\{\alpha_i\}}^{(s)} = \frac{2\pi}{M} \sum_{j=1}^L \sum_{i=1}^M w_j^{(P)} p^s E^{(N)}(p, \theta_j, \varphi_i; \mathbf{u}, T) \prod_{l=1}^s e_{ji\alpha_l}. \quad (23)$$

This allows us to use the *Gauss-Laguerre* quadrature [105–107] after changing the integration variable from p to $x \equiv p^2$ in Eq. (15). Since

$$\mathcal{M}_{\{\alpha_i\}}^{(s)} = \frac{n}{2} \int_0^\infty dx x^{1/2} e^{-x} \mathcal{F}(x; T) \mathcal{E}_{\{\alpha_i\}}^{(s)}(x; \mathbf{u}, T) \quad (24)$$

contains the term $x^{1/2}$, we expand

$$\mathcal{F}(x; T) \equiv e^x F(x; T) \quad (25)$$

with respect to the generalized Laguerre polynomials $L_\ell^{(1/2)}(x)$ [106,107] defined by Eq. (C2) in Appendix C

$$\mathcal{F}(x; T) = \sum_{\ell=0}^{K-1} \frac{\Gamma(\ell+1)}{\Gamma(\ell+3/2)} \mathcal{F}_\ell^{(1/2)}(T) L_\ell^{(1/2)}(x). \quad (26)$$

The order $K-1$ of this expansion must be greater than or equal to N because $\mathcal{E}_{\{\alpha_i\}}^{(s)}(x; \mathbf{u}, T)$ is a polynomial of order at most N in x and hence is orthogonal to all generalized Laguerre polynomials $L_\ell^{(1/2)}(x)$ of order $\ell > N$. For a given N , the *minimal* SLB model would have $K = N + 1$, but higher values of K can improve, for example, the accuracy with which boundary conditions are implemented, a matter upon which we elaborate in Appendix E. By virtue of the orthogonality relation (C5), the coefficients $\mathcal{F}_\ell^{(1/2)}(T)$ are derived using the explicit form (C2) of the Laguerre polynomials, as well as the definition (C3) of the Γ function

$$\begin{aligned} \mathcal{F}_\ell^{(1/2)}(T) &= \int_0^\infty dx x^{1/2} e^{-x} \mathcal{F}(x; T) L_\ell^{(1/2)}(x) \\ &= \int_0^\infty dx x^{1/2} F(x; T) L_\ell^{(1/2)}(x) \\ &= (2mT\pi)^{-D/2} \sum_{s=0}^{\ell} \frac{\Gamma(\ell+3/2)}{\Gamma(s+3/2)(\ell-s)!s!} \\ &\quad \times (-1)^s \int_0^\infty ds x^{s+1/2} e^{-x/2mT} \\ &= \frac{\Gamma(\ell+3/2)}{\ell!} \pi^{-D/2} \sum_{s=0}^{\ell} \frac{\ell!(-2mT)^s}{(\ell-s)!s!}. \end{aligned} \quad (27)$$

Since the sum in the last line of Eq. (27) above is the binomial expansion of $(1-2mT)^\ell$, we get

$$\mathcal{F}(x; T) = \pi^{-D/2} \sum_{\ell=0}^{K-1} (1-2mT)^\ell L_\ell^{(1/2)}(x). \quad (28)$$

The application of Gauss-Laguerre quadrature rules, presented in Appendix C, gives

$$\mathcal{M}_{\{\alpha_i\}}^{(s)} = \frac{n}{2} \sum_{k=1}^K w_k^{(L)} \mathcal{F}(x_k; T) \mathcal{E}_{\{\alpha_i\}}^{(s)}(x_k; \mathbf{u}, T), \quad (29)$$

where x_k , $1 \leq k \leq K$, $K \geq N+1$ are the roots of the generalized Laguerre polynomial $L_{N+1}^{(1/2)}(x)$ defined in Appendix C and

$$w_k^{(L)} = \frac{x_k \Gamma(K+3/2)}{K!(K+1)^2 [L_{K+1}^{(1/2)}(x_k)]^2} \quad (30)$$

are the corresponding quadrature weights.

III. THE SLB($N; K, L, M$) MODELS

According to the main result of the previous section, Eq. (29), the moments (3) of $f^{(\text{eq})}$, of order at most N , are exactly recovered by using a discrete set of equilibrium distribution functions

$$f_{kji}^{(\text{eq})} = n F_k E_{kji} \quad (31)$$

defined at time t in each node \mathbf{x} of a cubic lattice \mathcal{L} . Here n is the particle number density (5a) and the polynomial functions F_k and E_{kji} are defined as follows:

$$F_k = \frac{w_k^{(L)}}{M\sqrt{\pi}} \sum_{\ell=0}^{K-1} (1-2mT)^\ell L_\ell^{(1/2)}(p_k^2), \quad (32a)$$

$$E_{kji} = w_j^{(P)} E^{(N)}(\mathbf{p}_{kji}; \mathbf{u}, T), \quad (32b)$$

where

$$\mathbf{p}_{kji} = p_k \mathbf{e}_{ji}. \quad (33)$$

Due to the linearity of the Boltzmann equation, the quadrature weights w_k^L and w_j^P have been absorbed in the polynomial functions F_k and E_{kji} , respectively. The exact form of the generalized Laguerre polynomials $L_\ell^{(1/2)}(x)$, required for the construction of F_k , is discussed in Appendix A. The general form for $E^{(N)} \equiv E^{(N)}(\mathbf{p}; \mathbf{u}, T)$ is given by formula (11), having the pattern

$$\begin{aligned} E^{(N)} &= \left[1 - \frac{mu^2}{2T} + \frac{1}{2} \left(\frac{mu^2}{2T} \right)^2 - \frac{1}{3!} \left(\frac{mu^2}{2T} \right)^3 \right. \\ &\quad \left. + \frac{1}{4!} \left(\frac{mu^2}{2T} \right)^4 \right] + \frac{\mathbf{u} \cdot \mathbf{p}}{T} \left(1 + \frac{1}{2} \frac{\mathbf{u} \cdot \mathbf{p}}{T} \right) \\ &\quad \times \left[1 - \frac{mu^2}{2T} + \frac{1}{2} \left(\frac{mu^2}{2T} \right)^2 - \frac{1}{3!} \left(\frac{mu^2}{2T} \right)^3 \right] \\ &\quad + \frac{1}{3!} \left(\frac{\mathbf{u} \cdot \mathbf{p}}{T} \right)^3 \left(1 + \frac{1}{4} \frac{\mathbf{u} \cdot \mathbf{p}}{T} \right) \left[1 - \frac{mu^2}{2T} + \frac{1}{2} \left(\frac{mu^2}{2T} \right)^2 \right] \\ &\quad + \frac{1}{5!} \left(\frac{\mathbf{u} \cdot \mathbf{p}}{T} \right)^5 \left(1 + \frac{1}{6} \frac{\mathbf{u} \cdot \mathbf{p}}{T} \right) \left[1 - \frac{mu^2}{2T} \right] \\ &\quad + \frac{1}{7!} \left(\frac{\mathbf{u} \cdot \mathbf{p}}{T} \right)^7 \left(1 + \frac{1}{8} \frac{\mathbf{u} \cdot \mathbf{p}}{T} \right) + O(u^9). \end{aligned} \quad (34)$$

Equation (31) gives the equilibrium distribution functions $f_{kji}^{(\text{eq})}$ in the LB model of order N with Gauss quadrature in spherical coordinates, as well as the Cartesian components $p_{kji\alpha}$ ($\alpha = 1, 2, 3$) of the corresponding momentum vectors \mathbf{p}_{kji} ($1 \leq k \leq K$, $1 \leq j \leq L$, $1 \leq i \leq M$). The members of this family (hierarchy) of *spherical shell* LB models will be denoted SLB($N; K, L, M$).

Figure 1 shows the first four SLB($N; K, L, M$) models ($1 \leq N \leq 4$) in the hierarchy. All the models shown in this figure have the minimum number of momentum vectors for a given N . As discussed previously, the rules for choosing the values of K , L , and M for a given N are

$$K > N, \quad L > N, \quad M > 2N. \quad (35)$$

These rules ensure the exact recovery of all the moments of $f^{(\text{eq})}$ of order less than or equal to N . The value of N depends

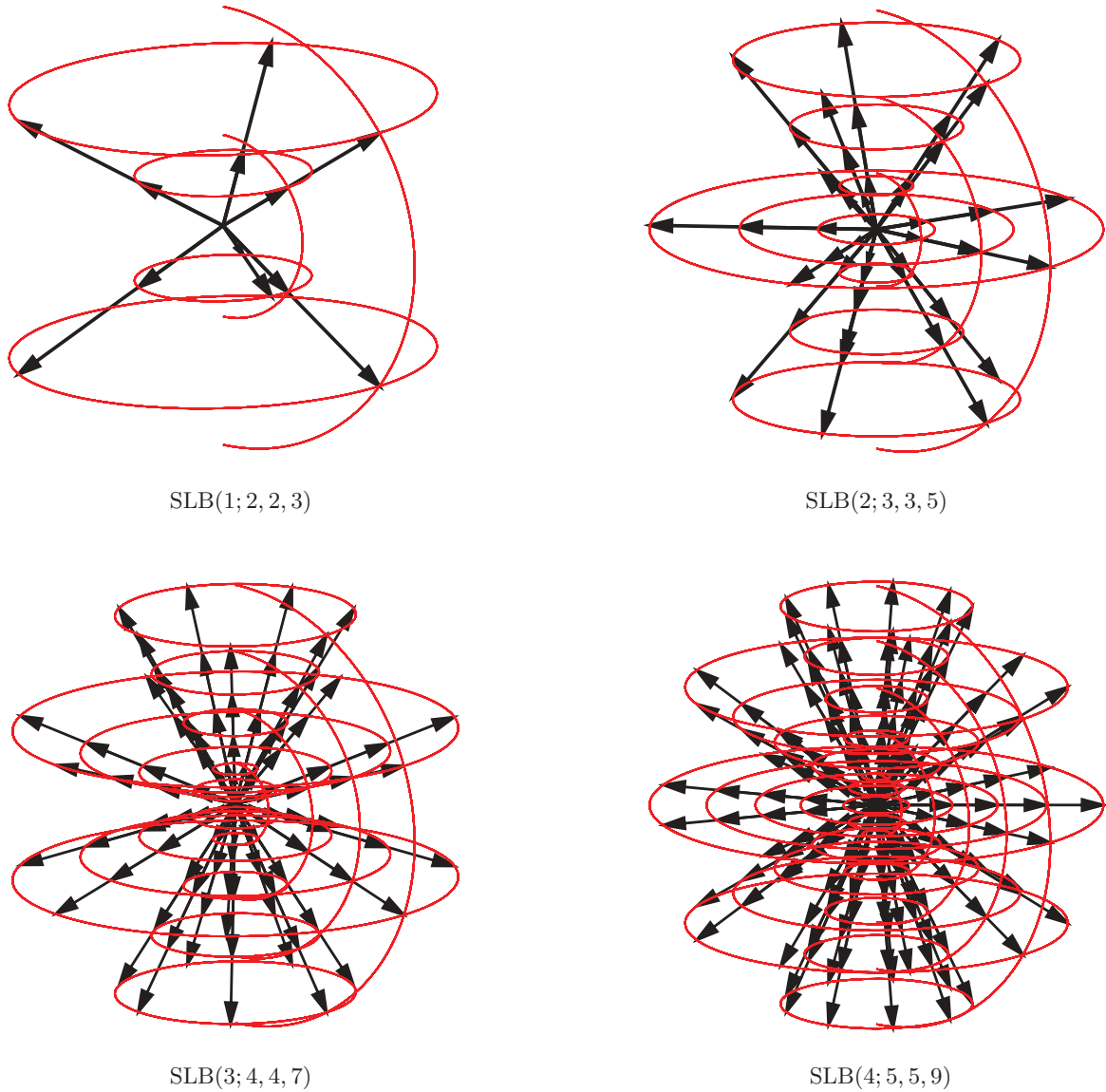


FIG. 1. (Color online) First four members of the *spherical shell* SLB family: $SLB(N; K, L, M)$ with $N = 1, \dots, 4$, $K = N + 1$, $L = N + 1$, $M = 2N + 1$.

on the physics one aims to capture. As long as conditions (35) are fulfilled, the values of K , L , and M can be increased arbitrarily. This will help increase the accuracy of simulation results when dealing with boundary conditions, as shall be discussed in Sec. **VIB**.

The resulting momentum space configuration of the $SLB(N; K, L, M)$ model has $K \times L \times M$ momentum vectors structured on K spherical shells situated at the distances $p_k = x_k^{1/2}$ ($k = 1, 2, \dots, K$) from the origin. According to Eq. (35), the minimum number of momentum vectors for a given value of N is $(N + 1)^2(2N + 1)$.

For $N = 1, 2, \dots, 8$ and $K = N + 1$, the roots x_k of the generalized Laguerre polynomials $L_K^{(1/2)}(x)$, as well as their associated weights $w_k^{(L)}$ can be found in Table **VI** of Appendix **A**. The weights $w_k^{(L)}$, which correspond to $p_k = \sqrt{x_k}$, are depicted in Fig. 2 for $N = 3, 4, \dots, 8$.

Each shell k ($k = 1, 2, \dots, K$) of the model $SLB(N; K, L, M)$ is a sphere of radius p_k . On this sphere

there are L circles situated on parallel planes $z_j = \cos(\theta_j)$ ($j = 1, 2, \dots, L$) perpendicular to the z axis. The values of z_j and their corresponding weights $w_j^{(P)}$ (calculated to machine precision for $L \leq 8$) are given in Table **V** of Appendix **B**. The circle defined by the intersection of plane j with the shell k contains the tips of M uniformly distributed momentum vectors \mathbf{p}_{kji} ($i = 1, 2, \dots, M$). The angle formed by the equally spaced projections of \mathbf{p}_{kji} and the x axis is given by the formula (18).

The value of the arbitrary offset angle ϕ becomes important when there are walls bounding the flow domain which are not perpendicular to the z axis. In this case, our preferred choice for ϕ is π/M , with M a multiple of 4. The reasons behind our choice are presented in Sec. **VII**. The arbitrariness of ϕ is a particular case of the symmetry of the discrete set of momentum vectors under arbitrary rotations, which include changes of the direction of the zenith (z) and/or the azimuth (x) axis of the spherical coordinate system.

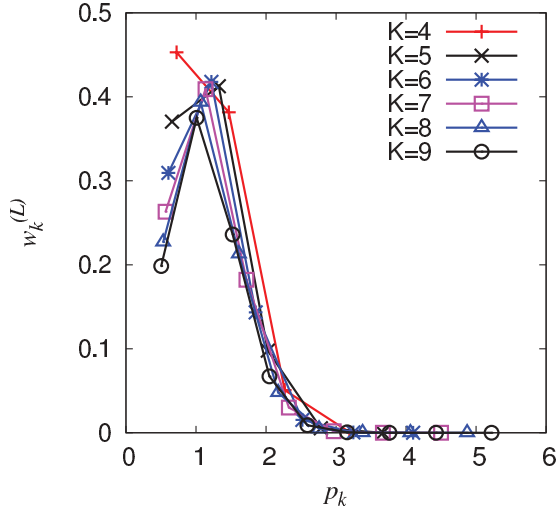


FIG. 2. (Color online) Weights $w_k^{(L)}$ associated to $p_k = \sqrt{x_k}$, for $K = 4, 5, \dots, 9$ ($k = 1, 2, \dots, K$).

IV. SHAKHOV COLLISION TERM AND CONSERVATION EQUATIONS

To ensure the right value of the Prandtl number for the ideal gas ($\text{Pr} = 2/3$), we use the Shakhov collision term [96–99] in the Boltzmann equation. This gives the following evolution equation for the distribution function $f \equiv f(\mathbf{x}, \mathbf{p}, t)$:

$$\partial_t f + \frac{p_\alpha}{m} \partial_\alpha f = -\frac{1}{\tau} [f - f^{(\text{eq})}(1 + \mathbb{S})] \quad (36)$$

(for simplicity, in this paper we consider that the fluid is not subjected to external forces). Here $\partial_t = \partial/\partial t$, $\partial_\alpha = \partial/\partial x_\alpha$, $\tau = \text{Kn}/n$ [78–82], and

$$\mathbb{S} = \frac{1 - \text{Pr}}{nT^2} q_\alpha \xi_\alpha \left[\frac{\xi^2}{(D+2)mT} - 1 \right], \quad (37)$$

$$q_\alpha = \frac{1}{2m^2} \delta_{\beta\gamma} \int d^D p f \xi_\alpha \xi_\beta \xi_\gamma, \quad (38)$$

where

$$\xi_\alpha = p_\alpha - mu_\alpha \quad (39)$$

are the Cartesian components of the peculiar momentum $\boldsymbol{\xi} = \mathbf{p} - m\mathbf{u}$. The widely used Bhatnagar-Gross-Krook (BGK) collision term [3,4] is retrieved as a particular case of the Shakhov collision term when \mathbb{S} is canceled by setting $\text{Pr} = 1$ in Eq. (37).

The following conditions need to be fulfilled to ensure the conservation of mass, momentum, and energy during interparticle collisions:

$$n = \int d^D p f = \int d^D p f^{(\text{eq})}(1 + \mathbb{S}), \quad (40a)$$

$$mnu_\alpha = \int d^D p f p_\alpha = \int d^D p f^{(\text{eq})}(1 + \mathbb{S}) p_\alpha, \quad (40b)$$

$$\begin{aligned} n \left(\frac{D}{2} T + \frac{1}{2} mu^2 \right) &= \frac{\delta_{\alpha\beta}}{2m} \int d^D p f p_\alpha p_\beta \\ &= \frac{\delta_{\alpha\beta}}{2m} \int d^D p f^{(\text{eq})} (1 + \mathbb{S}) p_\alpha p_\beta. \end{aligned} \quad (40c)$$

To get a better understanding of the effect of the Shakhov collision term on the conservation equations for mass, momentum, and energy, we first note that \mathbb{S} is proportional to the contraction of the third-order Hermite polynomial $\mathcal{H}_{\alpha\beta\gamma}^3(\boldsymbol{\xi})$ defined in Eq. (D1d)

$$\mathbb{S} \equiv \mathbb{S}(\boldsymbol{\xi}) = \frac{1 - \text{Pr}}{nT^2} \frac{\sqrt{mT}}{D+2} q_\alpha \delta_{\beta\gamma} \mathcal{H}_{\alpha\beta\gamma}^{(3)}(\boldsymbol{\xi}), \quad (41)$$

where $\xi_\alpha = (p_\alpha - mu_\alpha)/\sqrt{mT}$. According to the orthogonal relation Eq. (D3), \mathbb{S} is orthogonal to any polynomial of order less than or equal to 2 in $\boldsymbol{\xi}$, with respect to the weight function $\exp(-\boldsymbol{\xi}^2/2)$. Since the equilibrium distribution function $f^{(\text{eq})}$ defined by Eq. (4) is proportional to $\exp(-\boldsymbol{\xi}^2/2)$, one can easily see that \mathbb{S} is orthogonal to the following polynomials:

$$\begin{aligned} \mathcal{H}^{(0)}(\boldsymbol{\xi}) &= 1, \\ \sqrt{mT} \mathcal{H}_\alpha^{(1)}(\boldsymbol{\xi}) + mu_\alpha \mathcal{H}^{(0)}(\boldsymbol{\xi}) &= p_\alpha, \\ mT \mathcal{H}_{\alpha\beta}^{(2)}(\boldsymbol{\xi}) + \sqrt{m^3 T} [u_\alpha \mathcal{H}_\beta^{(1)}(\boldsymbol{\xi}) + u_\beta \mathcal{H}_\alpha^{(1)}(\boldsymbol{\xi})] \\ &+ (m^2 u_\alpha u_\beta + mT \delta_{\alpha\beta}) \mathcal{H}^{(0)}(\boldsymbol{\xi}) = p_\alpha p_\beta, \end{aligned}$$

and therefore does not contribute to the integrals in Eq. (40) above.

The pressure tensor $\pi_{\alpha\beta}$ is given by [80]

$$\pi_{\alpha\beta} = \frac{1}{m} \int d^D p f \xi_\alpha \xi_\beta = nT \delta_{\alpha\beta} + \sigma_{\alpha\beta}, \quad (42)$$

where $\sigma_{\alpha\beta}$ is the viscous stress tensor. Equations (38) and (42) may be written in an alternative form using the definition (39) of the peculiar momentum

$$\begin{aligned} \frac{1}{2m^2} \delta_{\beta\gamma} \int d^D p f p_\alpha p_\beta p_\gamma \\ = \left(\frac{D}{2} nT + \frac{1}{2} n u^2 \right) u_\alpha + q_\alpha + nT u_\alpha + \sigma_{\alpha\beta} u_\beta, \end{aligned} \quad (43)$$

$$\frac{1}{m} \int d^D p f p_\alpha p_\beta = mnu_\alpha u_\beta + nT \delta_{\alpha\beta} + \sigma_{\alpha\beta}. \quad (44)$$

This helps us derive the conservation equations by multiplying Eq. (36) with 1, p_α , or $p_\alpha p_\beta \delta_{\alpha\beta}/2m$ and subsequently integrating over the momentum space

$$\partial_t n + \partial_\alpha n u_\alpha = 0, \quad (45a)$$

$$\partial_t (mnu_\alpha) + \partial_\beta (mnu_\alpha u_\beta) + \partial_\beta (nT \delta_{\alpha\beta} + \sigma_{\alpha\beta}) = 0, \quad (45b)$$

$$\begin{aligned} \partial_t \left(\frac{D}{2} nT + \frac{1}{2} mnu^2 \right) + \partial_\alpha \left[u_\alpha \left(\frac{D}{2} nT + \frac{1}{2} mnu^2 \right) \right] \\ + \partial_\alpha q_\alpha + \partial_\alpha [u_\beta (nT \delta_{\alpha\beta} + \sigma_{\alpha\beta})] = 0. \end{aligned} \quad (45c)$$

The Chapman-Enskog method is currently used to derive the expressions for the transport coefficients (dynamic viscosity η and heat conductivity κ_T). According to this method, both f and ∂_t are expanded with respect to the small parameter

$\varepsilon \equiv \text{Kn}$

$$f = \sum_{l=0}^{\infty} \varepsilon^l f^{(l)}, \quad (46a)$$

$$\partial_t = \sum_{l=0}^{\infty} \varepsilon^l \partial_{t_l}, \quad (46b)$$

where $f^{(0)} \equiv f^{(\text{eq})}$ [2,3,80,108]. The use of Eq.(10) after the introduction of the expansion (46a) into Eqs. (38) and (42) gives

$$q_\alpha = \sum_{l=1}^{\infty} \varepsilon^l q_\alpha^{(l)}, \quad (47a)$$

$$\mathbb{S} = \sum_{l=1}^{\infty} \varepsilon^l \mathbb{S}^{(l)}, \quad (47b)$$

$$\sigma_{\alpha\beta} = \sum_{l=1}^{\infty} \varepsilon^l \sigma_{\alpha\beta}^{(l)}, \quad (47c)$$

with

$$q_\alpha^{(l)} = \frac{\delta_{\beta\gamma}}{2m^2} \int d^D p f^{(l)} \xi_\alpha \xi_\beta \xi_\gamma, \quad (48a)$$

$$\mathbb{S}^{(l)} = \frac{1 - \text{Pr}}{nT^2} q_\alpha^{(l)} \xi_\alpha \left[\frac{\xi^2}{(D+2)mT} - 1 \right], \quad (48b)$$

$$\sigma_{\alpha\beta}^{(l)} = \frac{1}{m} \int d^D p f^{(l)} \xi_\alpha \xi_\beta. \quad (48c)$$

Note that the expansions (47) above do not contain zero-order terms like $q_\alpha^{(0)}$ and $\sigma_{\alpha\beta}^{(0)}$. This is not surprising since there is no heat flux and no viscous stress in a fluid system at equilibrium.

After substituting the expansions (46), the evolution equation (36) can be solved separately for each power of ε . The zeroth- and first-order terms give the following equations:

$$\partial_{t_0} f^{(0)} + \frac{1}{m} p_\gamma \partial_\gamma f^{(0)} = \frac{1}{\tau} f^{(0)} \mathbb{S}^{(1)} - \frac{1}{\tau} f^{(1)}, \quad (49)$$

$$\partial_{t_1} f^{(0)} + \partial_{t_0} f^{(1)} + \frac{1}{m} p_\gamma \partial_\gamma f^{(1)} = \frac{1}{\tau} f^{(0)} \mathbb{S}^{(2)} - \frac{1}{\tau} f^{(2)}. \quad (50)$$

Since \mathbb{S} does not contribute to Eq. (40) we have, $\forall l > 0$

$$\int d^D p f^{(l)} = 0, \quad (51a)$$

$$\int d^D p f^{(l)} p_\alpha = 0, \quad (51b)$$

$$\frac{\delta_{\alpha\beta}}{2m} \int d^D p f^{(l)} p_\alpha p_\beta = 0. \quad (51c)$$

To get the conservation equations up to first order ($l = 1$) with respect to $\varepsilon \equiv \text{Kn}$, Eq. (49) can be used to express $f^{(1)}$ in the first-order equation (50) before performing the integration over the momentum space [3,80,108]

$$f^{(1)} = \tau f^{(0)} \left\{ \frac{D+2}{2mT} \xi_\beta \partial_\beta T - \frac{1}{2mT^2} \xi^2 \xi_\beta \partial_\beta T + \frac{1}{mT} \xi_\beta \xi_\gamma \partial_\gamma u_\beta - \frac{1}{DmT} \xi^2 \partial_\beta u_\beta \right\} + f^{(0)} \mathbb{S}^{(1)}. \quad (52)$$

TABLE I. The minimum values of N required by the Chapman-Enskog method for the retrieval of specific conservation equations (mass, momentum, and energy) at the Euler or Navier-Stokes-Fourier (NSF) level when using the BGK or Shakhov collision term.

	Euler		NSF	
	BGK	Shakhov	BGK	Shakhov
mass	1	3	2	4
momentum	2	4	3	5
energy	3	5	4	6

The above expression for $f^{(1)}$ can be obtained using the chain rule

$$\partial_t f^{(0)} = [(\partial_t n) \partial_n + (\partial_t u_\alpha) \partial_{u_\alpha} + (\partial_t T) \partial_T] f^{(0)}, \quad (53)$$

where $f^{(0)} \equiv f^{(\text{eq})}$ is given in Eq. (4). The time derivatives of n , u_α , and T are recovered from the zeroth-order conservation equations [i.e., Eq. (45)] with $q_\alpha = 0$ and $\sigma_{\alpha\beta} = 0$.

After the substitution of $f^{(1)}$ in the first-order evolution equation (50), all moments to be calculated involve the equilibrium distribution function only and have the general form defined in Eq. (3). This technique can easily be extended to higher orders ($l > 1$) of the Chapman-Enskog expansion, which become important as Kn increases. As stated in the introductory section, the investigation of fluid flow phenomena at increasing Knudsen number requires the recovery of higher-order moments, which may be achieved only by increasing N .

Table I lists the minimum value of N required for the recovery of specific conservation equations (mass, momentum, or energy), up to zeroth or first order with respect to ε (the so-called *Euler* and *Navier-Stokes-Fourier* levels, respectively). Choosing N greater than or equal to the values listed in Table I guarantees the exact recovery of the respective equation at the desired level, as indicated by the Chapman-Enskog expansion. The computer simulation results in Sec. VII A, as well as the theoretical analysis performed in Appendix F, which takes into account the particularities of the spherical quadratures, indicate that the actual minimum value for N required for the retrieval of the energy equation at the Navier-Stokes-Fourier (NSF) level with the SLB models can be smaller than the estimates in Table I.

At the Navier-Stokes-Fourier level, the viscous stress tensor and the heat flux are given by

$$\sigma_{\alpha\beta} = -\eta \left[\partial_\alpha u_\beta + \partial_\beta u_\alpha - \frac{2}{D} \delta_{\alpha\beta} (\partial_\gamma u_\gamma) \right], \quad (54a)$$

$$q_\alpha = -\kappa_T \partial_\alpha T, \quad (54b)$$

with the transport coefficients

$$\eta = \tau n T, \quad (55a)$$

$$\kappa_T = \frac{1}{\text{Pr}} \frac{D+2}{2m} \tau n T. \quad (55b)$$

The Prandtl number

$$\text{Pr} = \frac{c_p \eta}{\kappa_T}, \quad c_p = \frac{D+2}{2m} \quad (56)$$

is an adjustable parameter of the Shakhov collision term.

The architecture of the SLB models allows the total number of momenta in the corresponding velocity set to be optimized

according to symmetries of the moments required for the recovery of the physics governing the evolution of the system. A more thorough discussion can be found in Appendix A.

V. NUMERICAL SCHEME AND BOUNDARY CONDITIONS

The evolution equations (36) are numerically solved on a cubic lattice of spacing δs by projecting the discrete momenta \mathbf{p}_{kji} on the Cartesian axes and using the monitorized central difference (MCD) flux limiter scheme [40,43,60,109–116]. Let $\kappa_\alpha, \alpha \in \{1, 2, 3\}$ be the unit vectors of the Cartesian axes. To avoid possible confusion, in this section we do not use the implicit sum rule over the repeated index α and make explicit use of the sum symbol (Σ) when necessary.

For every distribution function $f_{kji}(\mathbf{x}, t)$, defined at node \mathbf{x} of the three-dimensional lattice at time t , we introduce the outgoing and incoming fluxes along the Cartesian axes [28–30,39,40,116]

$$\mathcal{F}_{kji\alpha}^{\text{out}}(\mathbf{x}, t) = f_{kji}(\mathbf{x}, t) + \frac{1}{2} \left(1 - \frac{|p_{kji\alpha}| \delta t}{\delta s} \right) \quad (57a)$$

$$\times [f_{kji\alpha}^{(+)}(\mathbf{x}, t) - f_{kji}(\mathbf{x}, t)] \Psi[\Theta_{kji\alpha}(\mathbf{x}, t)],$$

$$\mathcal{F}_{kji\alpha}^{\text{in}}(\mathbf{x}, t) = \mathcal{F}_{kji\alpha}^{\text{out}}[\mathbf{x} - \text{sgn}(p_{kji\alpha}) \delta s \kappa_\alpha, t]. \quad (57b)$$

In the equations above, $\Theta_{kji\alpha}(\mathbf{x}, t)$ denotes the *smoothness function*

$$\Theta_{kji\alpha}(\mathbf{x}, t) = \frac{f_{kji}(\mathbf{x}, t) - f_{kji\alpha}^{(-)}(\mathbf{x}, t)}{f_{kji\alpha}^{(+)}(\mathbf{x}, t) - f_{kji}(\mathbf{x}, t)} \quad (58)$$

and $\Psi[\Theta]$ is the *MCD flux limiter* [109–111]

$$\Psi[\Theta] = \begin{cases} 0, & \Theta \leq 0, \\ 2\Theta, & 0 \leq \Theta \leq 1/3, \\ (1 + \Theta)/2, & 1/3 \leq \Theta \leq 3, \\ 2, & 3 < \Theta. \end{cases} \quad (59)$$

For a given vector \mathbf{p}_{kji} , we used the *signum function* of real argument x

$$\text{sgn}(x) = \begin{cases} -1, & x < 0, \\ 0, & x = 0, \\ 1, & x > 0, \end{cases} \quad (60)$$

to specify the *forward and backward* distribution functions on the Cartesian axes

$$f_{kji\alpha}^{(+)}(\mathbf{x}, t) = f_{kji}[\mathbf{x} + \text{sgn}(p_{kji\alpha}) \delta s \kappa_\alpha, t], \quad (61a)$$

$$f_{kji\alpha}^{(-)}(\mathbf{x}, t) = f_{kji}[\mathbf{x} - \text{sgn}(p_{kji\alpha}) \delta s \kappa_\alpha, t]. \quad (61b)$$

After each time step δt , the distribution functions in node \mathbf{x} evolve according to

$$\begin{aligned} & f_{kji}(\mathbf{x}, t + \delta t) \\ &= f_{kji}(\mathbf{x}, t) - \sum_{\alpha} \frac{p_{kji\alpha}}{m} \frac{\delta t}{\delta s} [\mathcal{F}_{kji\alpha}^{\text{out}}(\mathbf{x}, t) - \mathcal{F}_{kji\alpha}^{\text{in}}(\mathbf{x}, t)] \\ & \quad - \frac{\delta t}{\tau} \{ f_{kji}(\mathbf{x}, t) - f_{kji}^{(\text{eq})}(\mathbf{x}, t) [1 + S_{kji}(\mathbf{x}, t)] \}. \end{aligned} \quad (62)$$

The application of the updating rule (62) in the bulk nodes of the lattice is straightforward. The same holds for lattice nodes where periodic boundary conditions apply. Special attention

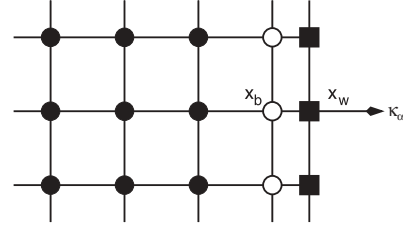


FIG. 3. Diffuse reflection boundary conditions: •, bulk nodes; ○, boundary nodes; ■, wall nodes.

should be paid when applying the updating rule (62) in the nodes located near the solid walls bounding the flow domain.

Let us consider a plane wall perpendicular to the Cartesian axis α . For convenience, we refer to the case in Fig. 3, where the unit vector normal to the wall (χ) has the same direction as the unit vector κ_α ($\chi \equiv \kappa_\alpha$). The wall is located at the distance $\delta s/2$ outside the boundary nodes, in the direction of κ_α . We focus our attention on the boundary node \mathbf{x}_b in Fig. 3 and note that Eq. (57) cannot be used to compute the outgoing fluxes $\mathcal{F}_{kji\alpha}^{\text{out}}(\mathbf{x}_b, t)$ when $p_{kji\alpha} > 0$, nor the incoming fluxes $\mathcal{F}_{kji\alpha}^{\text{in}}(\mathbf{x}_b, t)$ when $p_{kji\alpha} < 0$. Following [116], we set

$$\begin{aligned} \mathcal{F}_{kji\alpha}^{\text{out}}(\mathbf{x}_b, t) &= f_{kji}(\mathbf{x}_b, t) + \frac{1}{2} \left(1 - \frac{|p_{kji\alpha}| \delta t}{\delta s} \right) \\ & \quad \times [f_{kji}(\mathbf{x}_b, t) - f_{kji\alpha}^{(-)}(\mathbf{x}_b, t)] \end{aligned} \quad (63)$$

for $p_{kji\alpha} > 0$. According to the *diffuse reflection* concept [78–82], fluid particles reflected at time t in node \mathbf{x}_w on the wall follow the Maxwell distribution function $f^{(\text{eq})}(\mathbf{p}; n_w, \mathbf{u}_w, T_w)$, where $\mathbf{u}_w \equiv \mathbf{u}_w(\mathbf{x}_w, t)$ is the wall velocity and $T_w \equiv T_w(\mathbf{x}_w, t)$ is the local wall temperature (this quantity may vary along the wall, as considered in [117]). The density $n_w \equiv n_w(\mathbf{x}_w, t)$ is determined by requiring that the total particle flux in node \mathbf{x}_w vanishes in the direction normal to the wall [29,30,61,100,114–118]

$$n_w = \frac{\int_{\mathbf{p} \cdot \chi > 0} f(\mathbf{x}_w, t) \mathbf{p} \cdot \chi d^D p}{(\beta_w / \pi)^{D/2} \int_{\mathbf{p} \cdot \chi < 0} e^{-\beta_w (\mathbf{p} - m \mathbf{u}_w)^2} \mathbf{p} \cdot \chi d^D p}, \quad (64)$$

where $\beta_w = 1/2mT_w$. After replacing the integrals in the equation above with sums over the corresponding elements of the discretized momentum space and observing that the normal component of the incoming flux in node \mathbf{x}_w is identical to the outgoing flux in the boundary node \mathbf{x}_b of the lattice [116], we get

$$n_w = - \frac{\sum_{p_{kji\alpha} > 0} \mathcal{F}_{kji\alpha}^{\text{out}}(\mathbf{x}_b, t)}{\sum_{p_{kji\alpha} < 0} F_k(T_w) E_{kji}(\mathbf{u}_w, T_w) p_{kji\alpha}}. \quad (65)$$

This allows us to define the incoming particle flux in the boundary node \mathbf{x}_b , for $p_{kji\alpha} < 0$

$$\mathcal{F}_{kji\alpha}^{\text{in}}(\mathbf{x}_b, t) = -n_w F_k(T_w) E_{kji}(\mathbf{u}_w, T_w) p_{kji\alpha} \quad (66)$$

and ensures that the updating procedure (62) can be applied for all lattice nodes in the flow domain. As shown in [116], this procedure is of second order with respect to the lattice spacing δs .

VI. COMPUTER RESULTS

To illustrate the characteristics of the SLB models introduced in this paper we consider the problem of Couette flow between two parallel plates perpendicular to the z axis, located at $z_b = -0.5$ and $z_t = 0.5$, respectively. The plates have equal temperature $T_w(x, y, z_b) = T_w(x, y, z_t) = T_w = 1.0$ and move in opposite directions along the y axis with speed u_w such that $\mathbf{u}_w(x, y, z_b) = (0, 0, -u_w)$ and $\mathbf{u}_w(x, y, z_t) = (0, 0, u_w)$. To compare our computer simulation results to the direct simulation Monte Carlo (DSMC) results reported in [86,119], in this paper we use two values of u_w , namely 0.42 and 0.63. Computer simulations were done on a cubic lattice

with 100 nodes in the z direction and 2 nodes in the x and y directions where periodic conditions apply. The lattice spacing had the value $\delta s = 1/100$ and the time step was set to $\delta t = 10^{-4}$.

Throughout this section we consider only SLB models with $N = 6, K > N, L > N$, and $M = 13$. These models guarantee the recovery of moments up to order 6 of the equilibrium distribution function and thus unambiguously recover the Navier-Stokes-Fourier equations with both Shakhov and BGK collision terms. In Sec. VII we shall address the problem of optimizing these models by choosing smaller values for N, K, L and M , permissible because of the isotropy properties

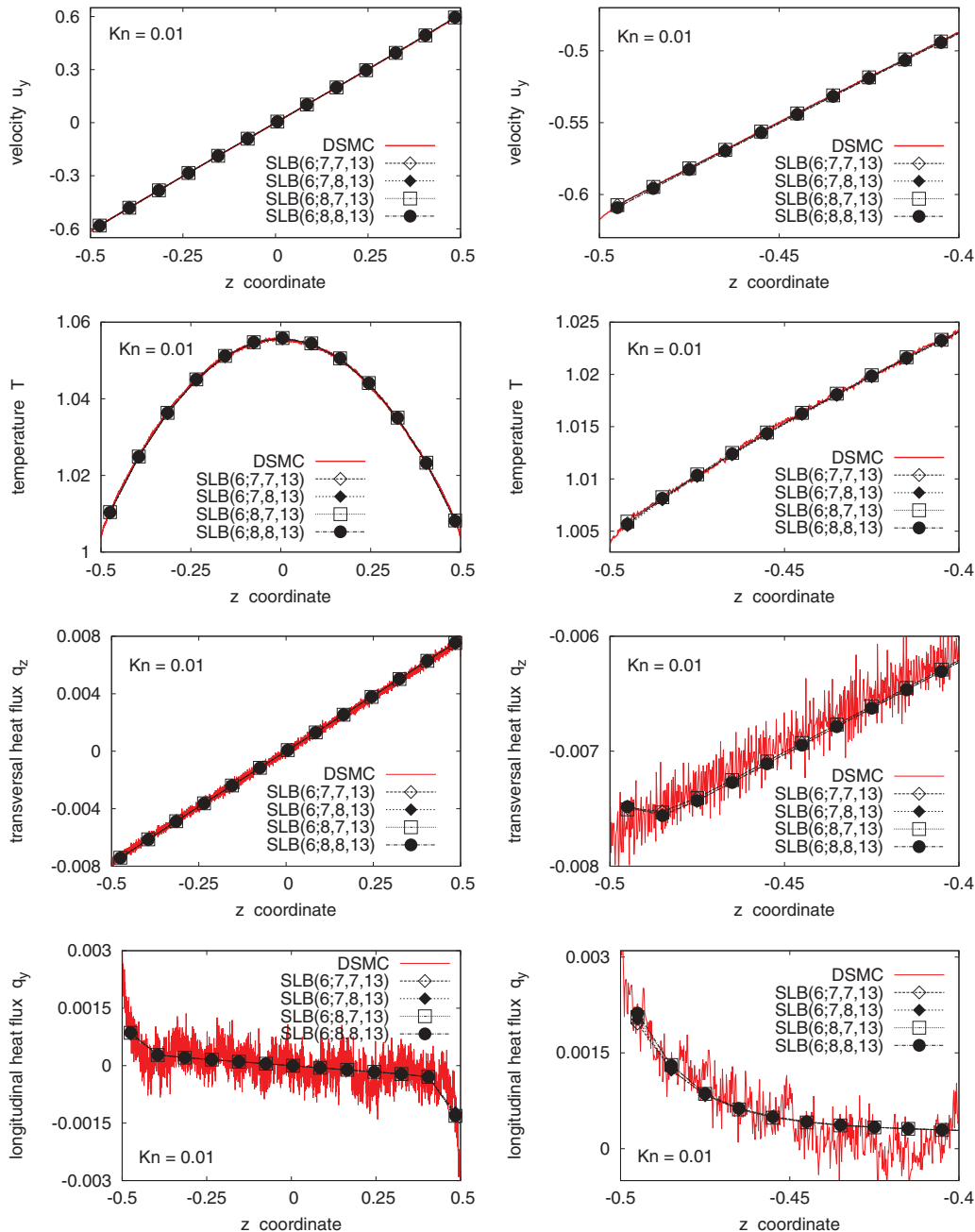


FIG. 4. (Color online) Stationary profiles (longitudinal fluid velocity u_y , temperature T , transversal heat flux q_z , longitudinal heat flux q_y) across the flow channel in Couette flow at $Kn = 0.01$ (Shakhov collision term; $T_w = 1.0$; $u_w = 0.63$).

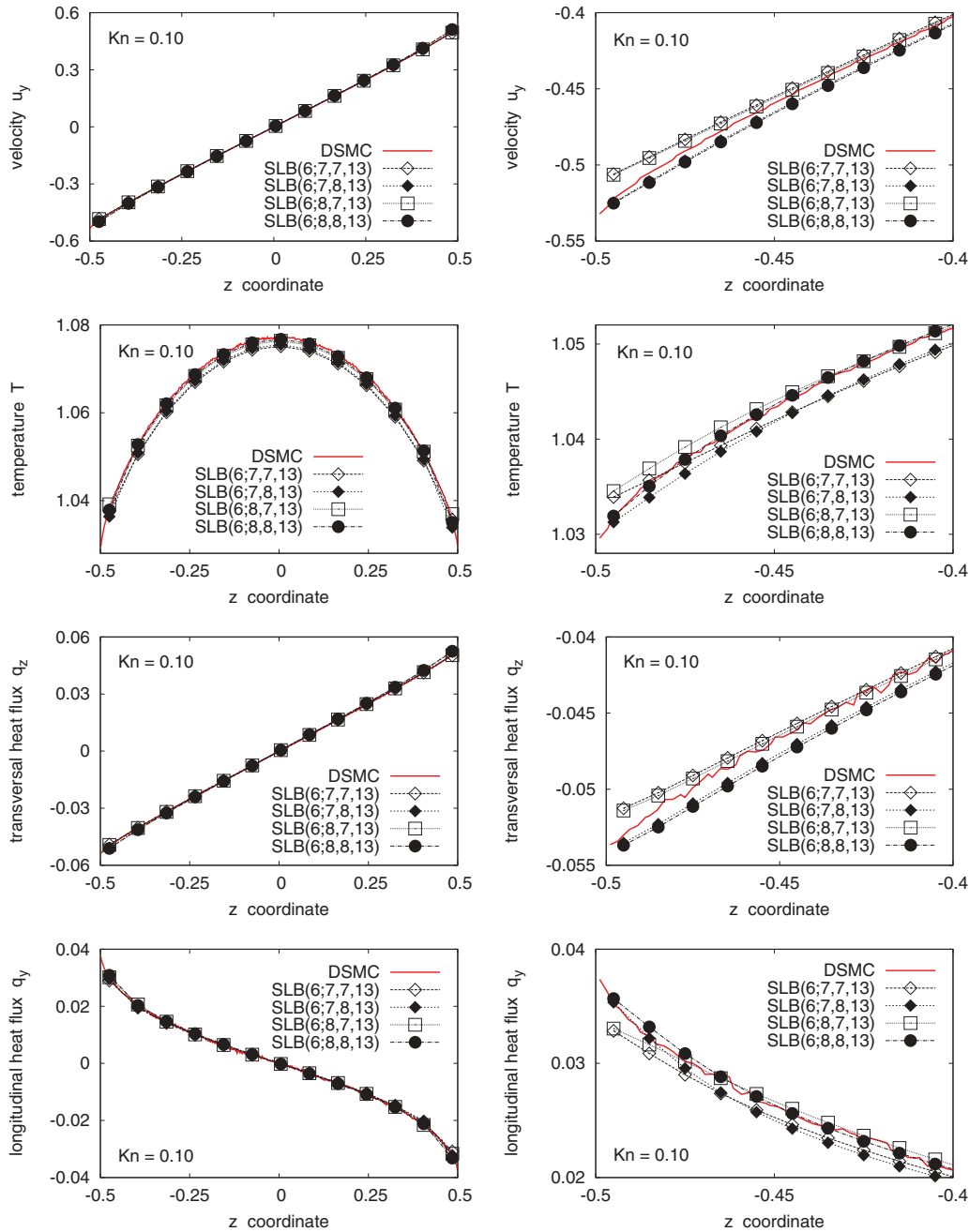


FIG. 5. (Color online) Stationary profiles (longitudinal fluid velocity u_y , temperature T , transversal heat flux q_z , longitudinal heat flux q_y) across the flow channel in Couette flow at $Kn = 0.10$ (Shakhov collision term; $T_w = 1.0$; $u_w = 0.63$).

of the particular moments necessary for the recovery of the conservation equations at the desired level.

A. Preliminary investigations

Figures 4 through 6 show the results of computer simulations carried out with the models SLB(6;7,7,13), SLB(6;7,8,13), SLB(6;8,7,13), and SLB(6;8,8,13) for three values of Kn (0.01, 0.10, and 0.50). The Shakhov collision term was used in these simulations and the results are compared to DSMC results for hard sphere molecules [85–88,119]. As seen in Figs. 4 through 6, good agreement between the DSMC results and the four SLB models is observed up to

$Kn = 0.10$ (Fig. 5). This value of Kn is generally recognized as the upper limit of the *slip flow regime*, where one can still rely on the Navier-Stokes-Fourier equations provided appropriate boundary conditions are considered to account for the slip velocity and the temperature jump at the walls [78–83]. The slip velocity, the temperature jump, as well as the Knudsen layer where the velocity profile is nonlinear and a longitudinal heat flux is generated, are well captured at $Kn = 0.01$ and $Kn = 0.10$ with the four SLB models, despite the large value $u_w = 0.63$ of the walls' speed. Although the results of computer simulations conducted with the four models SLB(6; $K, L, 13$), $K = 7, 8$, $L = 7, 8$ stand very close at $Kn = 0.10$, this is no longer valid as Kn is increased

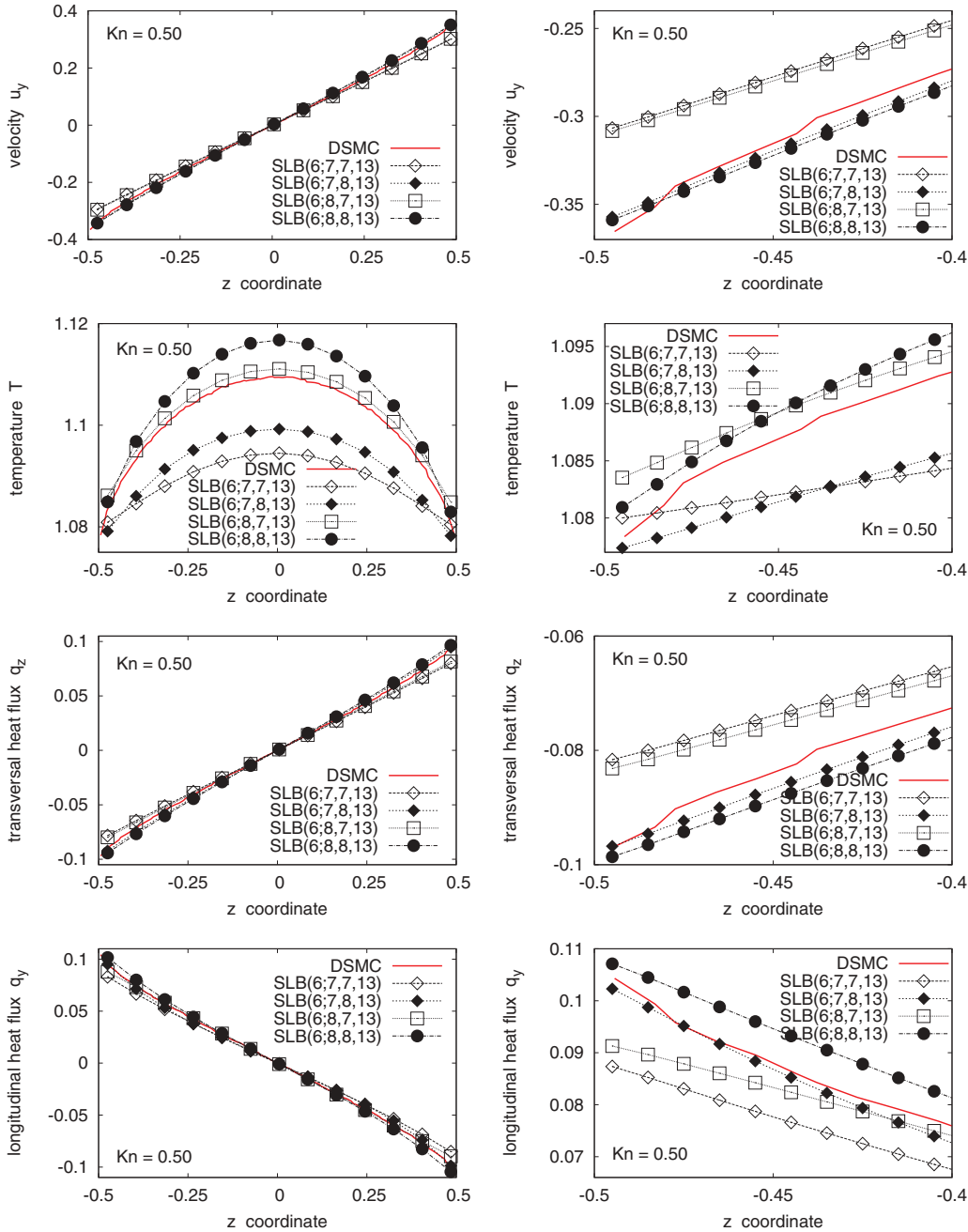


FIG. 6. (Color online) Stationary profiles (longitudinal fluid velocity u_y , temperature T , transversal heat flux q_z , longitudinal heat flux q_y) across the flow channel in Couette flow at $Kn = 0.50$ (Shakhov collision term; $T_w = 1.0$; $u_w = 0.63$).

further. For $Kn = 0.50$, (Fig. 6), the two $SLB(6; K, 8, 13)$ models ($K = 7, 8$) still produce quite identical profiles for the velocity and the transversal heat flux. These profiles are closer to the DSMC results than the profiles produced by the $SLB(6; K, 7, 13)$ models.

Surprisingly, the temperature profiles produced by the four models $SLB(6; K, L, 13)$, $K = 7, 8$, $L = 7, 8$ differ significantly for $Kn = 0.5$, even for $L = 8$. As suggested by other authors [29,71,101,102,120], this behavior originates from the half-space integrals involved in the implementation of the diffuse reflection boundary condition, Eq. (64). The recovery of the half-space integrals for the Couette flow

with the walls perpendicular to the z axis is discussed in Appendix E. If the discrete set of momentum vectors of a specific LB model includes vectors that are parallel to the wall, the corresponding distribution functions do not contribute to the sums in Eq. (65), generating larger errors in the evaluation of the half-space integrals in Eq. (64), with respect to the case when the discrete set of momentum vectors does not include such vectors [29,71,101,102,120,121]. When the z axis is perpendicular to the channel walls, there are momentum vectors parallel to the walls in models $SLB(N; K, L, M)$ when L is odd (Fig. 1). For this reason, models $SLB(6; K, 7, 13)$ give less accurate results than models $SLB(6; K, 8, 13)$, especially

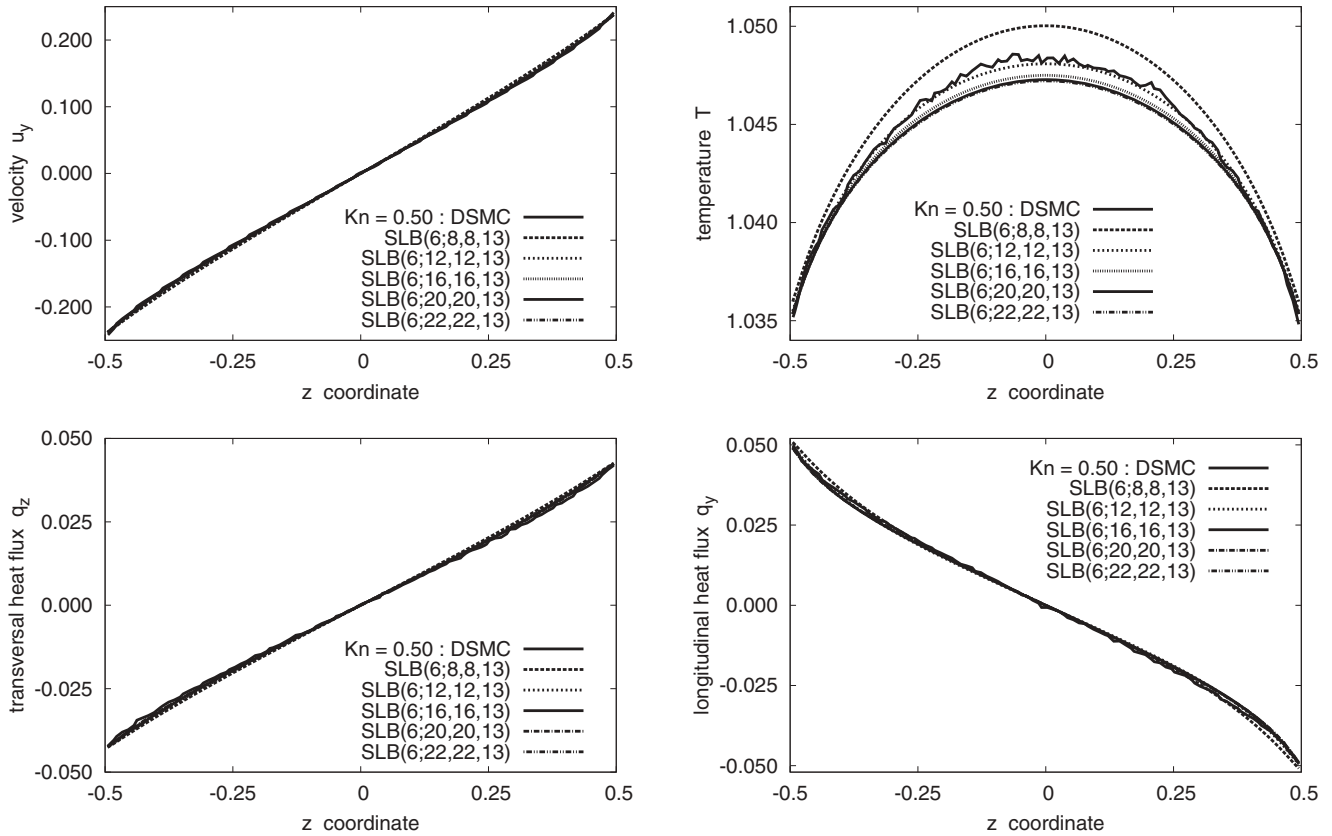


FIG. 7. Stationary profiles (longitudinal fluid velocity u_y , temperature T , transversal heat flux q_z , longitudinal heat flux q_y) across the channel in Couette flow at $\text{Kn} = 0.50$ ($T_w = 1.0$; $u_w = 0.42$) recovered with various quadrature orders $K = L$.

near the walls (Fig. 6). Moreover, as seen in Figs. 4 through 6, the accuracy decreases as Kn increases.

B. Effect of quadrature orders K, L on the accuracy of the results

To get further insight on the effect of various values of the Laguerre and Legendre quadrature orders K, L on the accuracy of the results, we conducted three series of simulations with

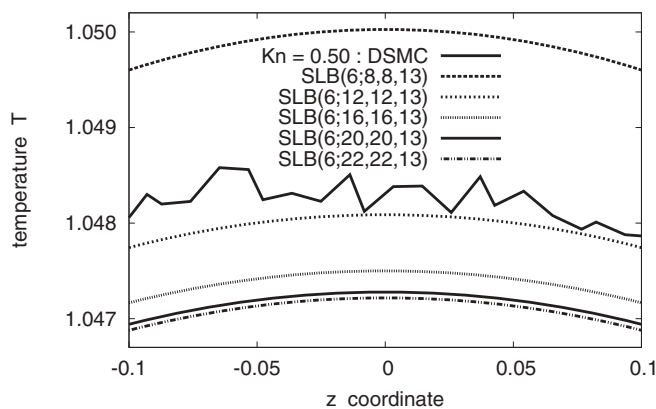


FIG. 8. Stationary profiles of fluid temperature T in the central region of the channel in Couette flow at $\text{Kn} = 0.50$ ($T_w = 1.0$; $u_w = 0.42$) recovered with various quadrature orders $K = L$.

models $\text{SLB}(6, K, L, 13)$. These simulations of Couette flow were done at $\text{Kn} = 0.50$ with wall temperature $T_w = 1.0$ and speed $u_w = 0.42$.

Figure 7 shows the results for the first series, when L is even and $K = L$. These results are compared to the corresponding DSMC results [85–88,119]. As observed during the preliminary investigations (Figs. 4 to 6), the longitudinal velocity profiles u_y , as well as the transversal and longitudinal heat flux profiles q_z and q_y are very close to the corresponding DSMC profiles (Fig. 7). Apparently, these profiles are less sensitive to changes in K and L than the temperature profile. Although all profiles converge (become closer) when increasing the quadrature orders, only the temperature profile shows large variations. The convergence of the temperature profiles at $\text{Kn} = 0.50$ is more clearly seen in Fig. 8, where the profiles are plotted in the central region of the channel. The convergence process of the temperature profiles at various values of Kn may be seen also in Fig. 14 (Sec. VIC), where we compare the SLB results obtained with the BGK and Shakhov collision terms by plotting the dependence of the temperature value in the center of the channel ($z = 0$) with respect to the quadrature order K for even values of K ($K = L$).

In the second series of simulations, we used a constant value for the Laguerre quadrature order ($K = 22$) and varied the Legendre quadrature order up to $L = 22$. Similarly, in the third series of simulations we varied the value of K while keeping $L = 22$. The results of these simulations (velocity and temperature profiles near the left wall) are shown in Figs. 9 and 10, respectively.

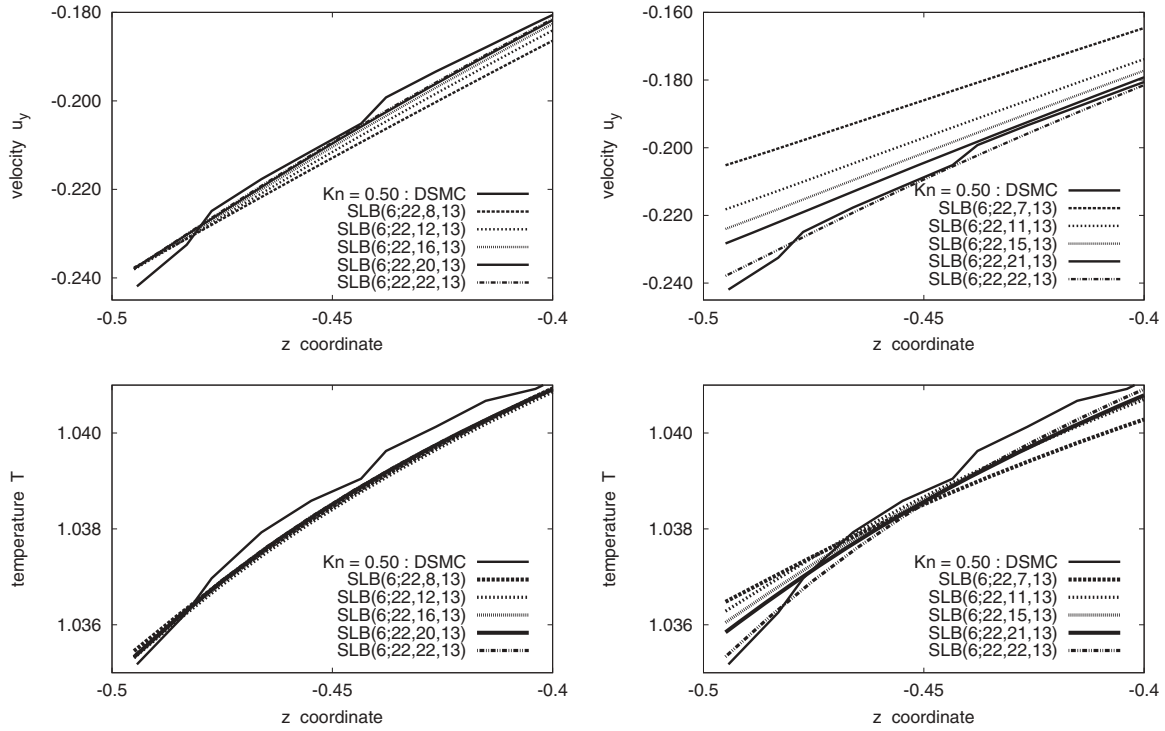


FIG. 9. Stationary profiles (longitudinal fluid velocity u_y and temperature T) near the left wall in Couette flow at $Kn = 0.50$ ($T_w = 1.0$; $u_w = 0.42$), for $K = 22$ and variable L (results corresponding to even and odd values of L are plotted separately).

For $K = 22$, the convergence process of the velocity and temperature profiles near the wall is very fast for even values of L and the profiles are quite well superposed for $L \geq 16$. For

$K = 22$ and odd values of L , the convergence process near the wall is much slower and still not achieved up to $L = 21$. However, in the central region of the channel the convergence

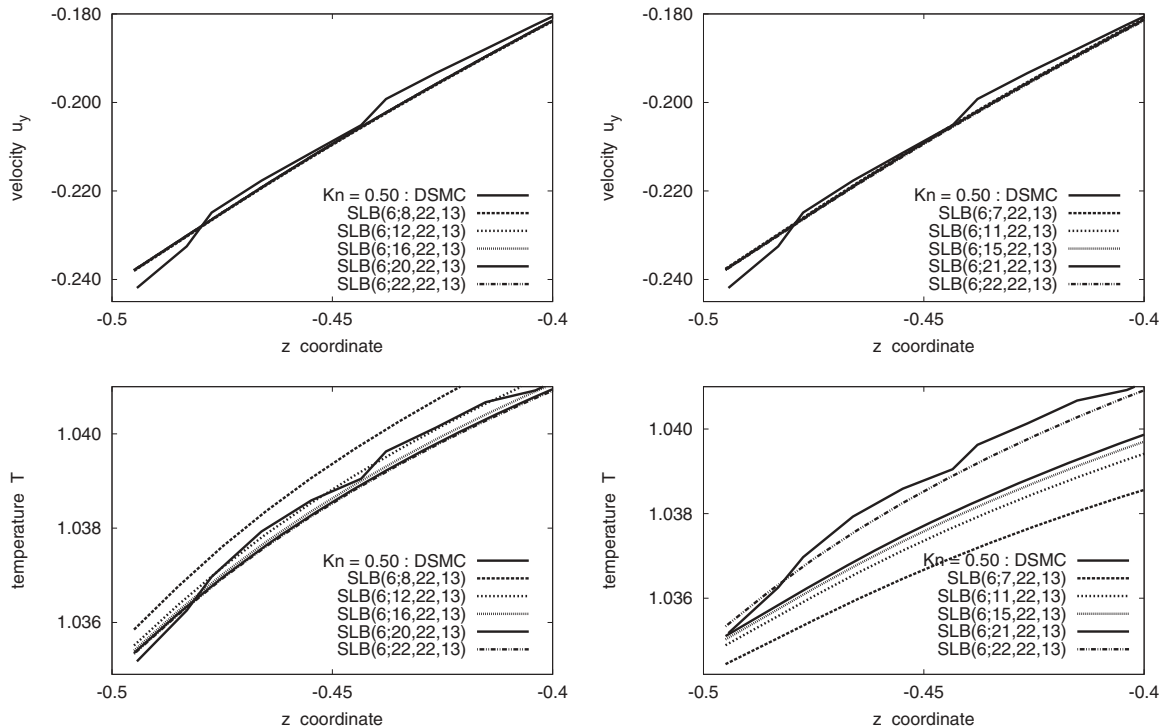


FIG. 10. Stationary profiles (longitudinal fluid velocity u_y and temperature T) near the left wall in Couette flow at $Kn = 0.50$ ($T_w = 1.0$; $u_w = 0.42$), for $L = 22$ and variable K (results corresponding to even and odd values of K are plotted separately).

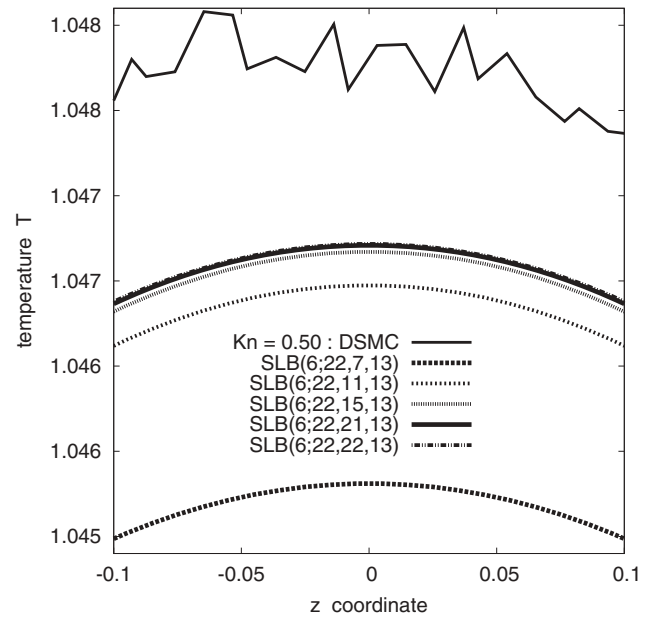
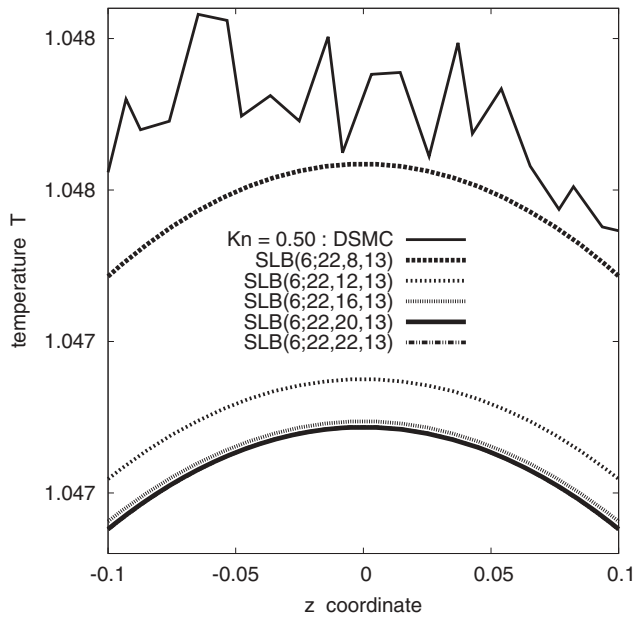


FIG. 11. Stationary profiles of fluid temperature T in the central region of the channel in Couette flow at $\text{Kn} = 0.50$ ($T_w = 1.0$; $u_w = 0.42$), for $K = 22$ and various values of L (results corresponding to even and odd values of L are plotted separately).

process of the temperature profiles is practically achieved for $L \geq 16$ regardless of the parity of L (Fig. 11).

The results of the third series of simulations show a somewhat different behavior. As seen in Fig. 10, the velocity profiles are well superposed for $L = 22$ and all tested values of K (even or odd). Apparently, the convergence of the temperature profiles is achieved faster for even values of K and slower for odd values (Fig. 12).

C. Comparison between SLB results obtained with the BGK and Shakhov collision terms

Figure 13 shows the simulation results obtained with the model SLB(6; 22, 22, 13) using the BGK and Shakhov collision terms. In these simulations, the Couette flow with $T_w = 1.0$ and $u_w = 0.42$ was considered at three values of Kn (0.05, 0.10, and 0.50). A comparison to DSMC results for hard sphere molecules [85–88, 119] reveals that both BGK and Shakhov

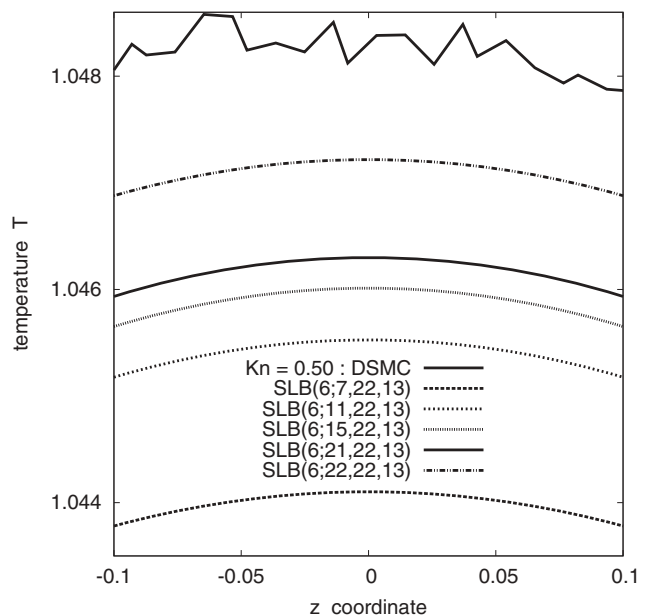
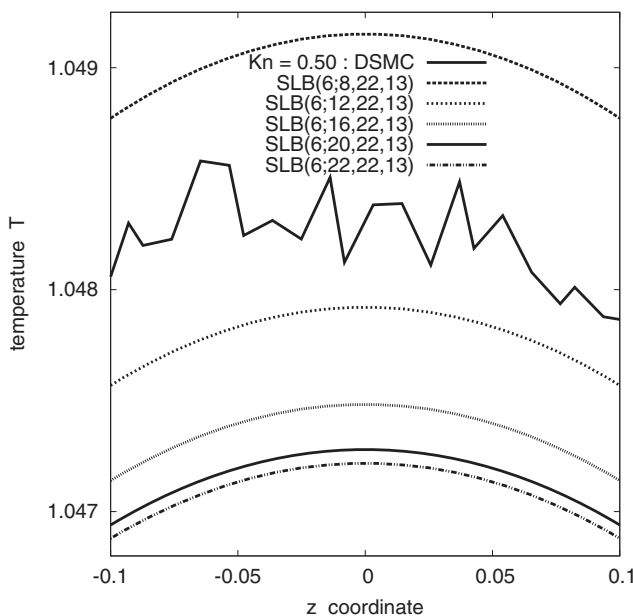


FIG. 12. Stationary profiles of fluid temperature T in the central region of the channel in Couette flow at $\text{Kn} = 0.50$ ($T_w = 1.0$; $u_w = 0.42$), for $L = 22$ and various values of K (results corresponding to even and odd values of L are plotted separately).

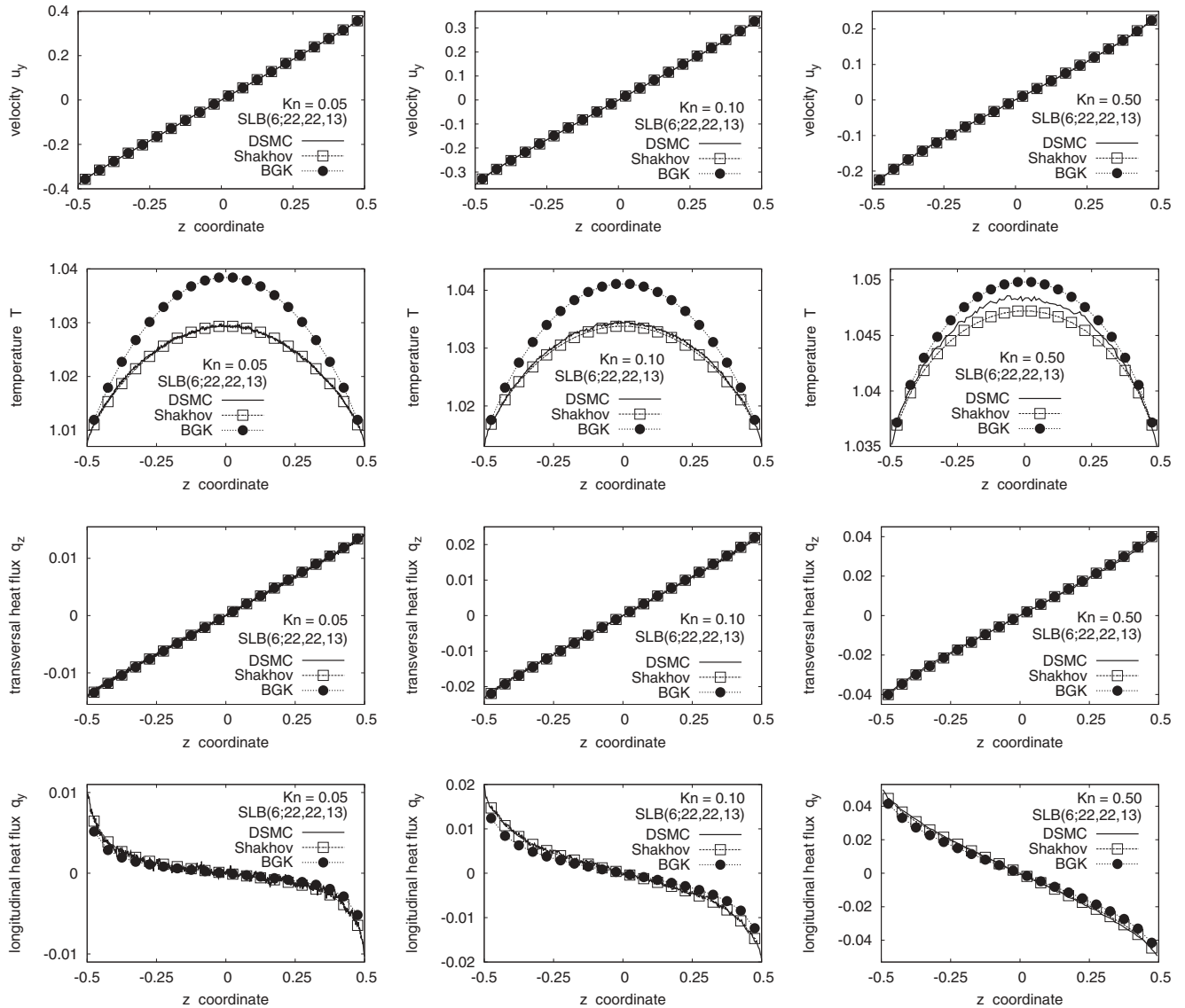


FIG. 13. Comparison between SLB results obtained with the BGK and Shakhov collision terms for Couette flow at three values of the Knudsen number Kn ($T_w = 1.0$; $u_w = 0.42$).

collision terms give good results for the velocity profile, as well as for the transversal heat flux. The longitudinal heat flux is better captured with the Shakhov collision term. For given Kn and $K = L$, the temperature values in the center of the channel converge when increasing the Gauss-Laguerre quadrature order K , as seen in Fig. 14.

For a given Kn , the temperature values recovered using the BGK collision term are always higher than the corresponding values recovered with the Shakhov collision term. This is due to the larger value of the Prandtl number achieved with the BGK collision term [3,108,116]. Although the DSMC and Shakhov temperature profiles agree very well at the Navier-Stokes level (up to $Kn \simeq 0.1$), the Shakhov temperature profile sets below the DSMC temperature profile when Kn is increased further. A similar behavior was previously reported during computer simulations done with Mieussens' *discrete velocity model* [84,122–124] using the so-called ellipsoidal statistical collision term (ES-BGK). As discussed in [84,122],

the simplified collision terms used in computer models do not account for all the features of the collision integral in the Boltzmann equation. The particularities of each collision term are responsible for the differences observed in the simulation results when exploring a large range of Kn . Their exploration is beyond the scope of this work, which is devoted to the introduction of LB models based on Gauss quadratures when the spherical coordinate system is used in the momentum space.

D. Effect of time step δt and lattice spacing δs

The Couette flow simulations reported in this section were done on a cubic lattice with 100 nodes in the z direction and 2 nodes in the x and y directions where periodic conditions apply. The time step had the value $\delta t = 10^{-4}$ and the lattice spacing was set to $\delta s = 1/100$. Equation (62) was used to update the distribution functions in each lattice node, after

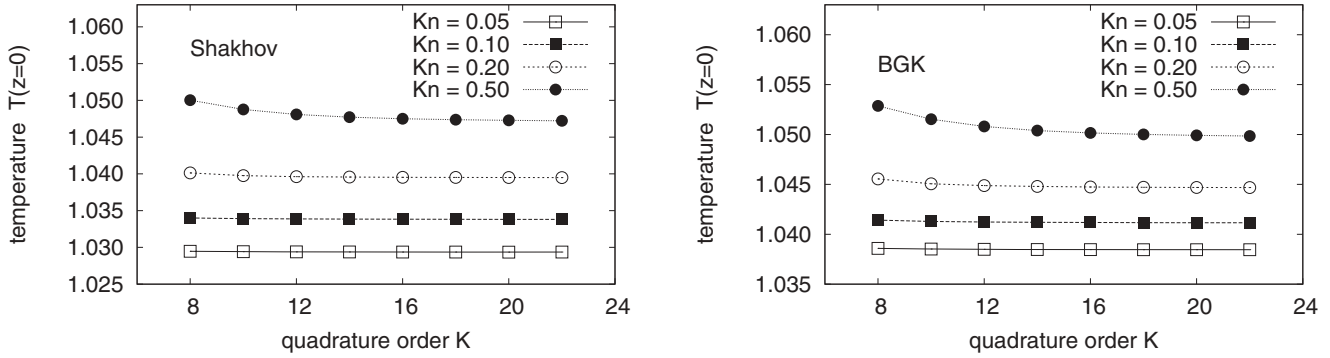


FIG. 14. The convergence of the temperature values with respect to quadrature order K in the center of the channel ($z = 0$) for Couette flow at various values of the Knudsen number Kn ($T_w = 1.0$; $u_w = 0.42$) when using the Shakhov and BGK collision terms. Results were obtained using the models $SLB(6; K, L = K, 13)$ with $K \in \{8, 10, 12, 14, 16, 18, 20, 22\}$.

each time step. The numerical scheme this equation is based on is of first order with respect to the time step δt and of second order with respect to the lattice spacing δs [116]. This is seen in Figs. 15 and 16, where we plotted the dependence of the fluid temperature in the center of the channel versus δt and δs for two values of Kn . The minor change of the temperature value noticed when δt and δs become one order of magnitude smaller support the values we selected for the simulations reported in this paper ($\delta t = 10^{-4}$ and $\delta s = 1/100$).

VII. OPTIMAL SLB MODELS FOR COUETTE FLOW AT THE NAVIER-STOKES-FOURIER LEVEL ($Kn < 0.1$)

As discussed in Sec. III, for a given order N of the series expansion in Eq. (11) the minimal SLB model (i.e., the model that has the smallest number of momentum vectors) is $SLB(N; N + 1, N + 1, 2N + 1)$. To ensure the accuracy of the simulation results, as well as the lowest computational costs (computational time and memory requirements), it is important to choose the right model in the SLB hierarchy when investigating a particular flow problem. Following the experience gained from the simulations reported in the previous section, we will discuss here the choice of optimal SLB models for the simulation of Couette flow between parallel plates perpendicular to the z axis. As seen in Sec. VIB, the quadrature orders K, L , and the computational costs required to get accurate results using the implementation of the diffuse reflection boundary conditions introduced in Sec. V increase substantially when going beyond $Kn = 0.1$. For this reason, in

this section we will restrict our analysis to the slip flow regime ($Kn < 0.1$), where the Navier-Stokes-Fourier (NSF) level is still applicable [78–83].

A. Finding the minimum value of the order N of the series expansion Eq. (34)

According to Table I, the recovery of the flow equations at the NSF level would require the moments of the equilibrium distribution function up to order 4 or 6, depending on the collision term (BGK or Shakhov). To check this, we first conducted Couette flow simulations at $Kn = 0.100$ using the minimal models $SLB(N; N + 1, N + 1, 2N + 1)$, as well as models $SLB(N; 8, 8, 15)$, for $N = 2, 3, \dots, 7$. The models $SLB(N; 8, 8, 15)$ were considered in this section to keep all simulation parameters fixed, except the order N of the series expansion, Eq. (11).

Stationary profiles of velocity and temperature near the left wall, as well as temperature profiles across the channel are plotted in Figs. 17 and 18, respectively. Apparently, the results obtained with the minimal models $SLB(N; N + 1, N + 1, 2N + 1)$ depend strongly on N . These results seem to converge when N , and hence the number of momentum vectors in the models $SLB(N; N + 1, N + 1, 2N + 1)$, increases. Contrastingly, the $SLB(N; 8, 8, 15)$ models, which all have the same number of momentum vectors, produce results that appear to be well superposed, except for $N = 2$. As noticed in Sec. VIB, the quadrature orders K, L should be high enough to ensure the accurate implementation of the diffuse reflection boundary

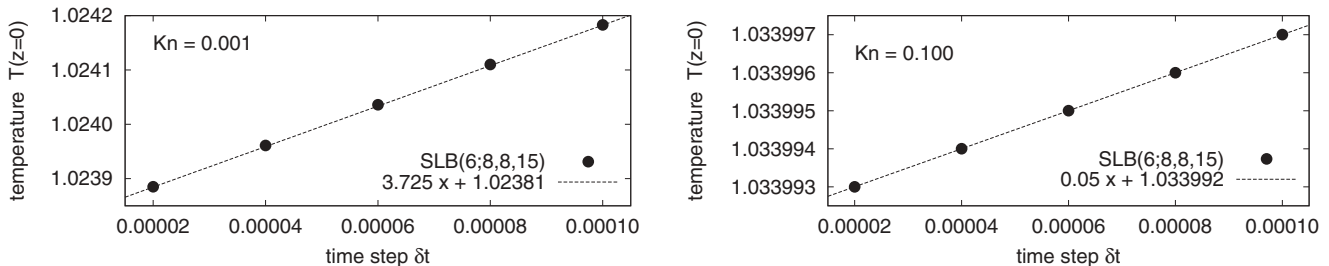


FIG. 15. Effect of time step δt on the temperature value in the center of the channel ($z = 0$) for Couette flow at $Kn = 0.001$ and $Kn = 0.100$ ($u_w = 0.42$; $T_w = 1.0$, $\delta s = 0.01$). The results were obtained using the model $SLB(6; 8, 8, 15)$ with the Shakhov collision term.

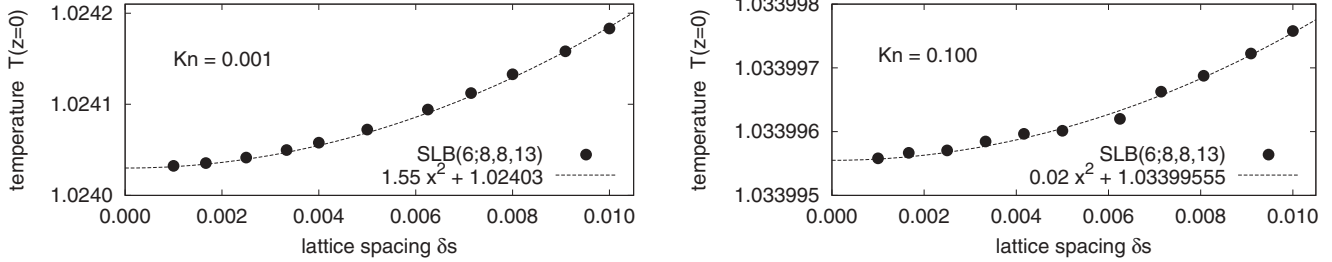


FIG. 16. Effect of lattice spacing δs on the temperature value in the center of the channel ($z = 0$) for Couette flow at $\text{Kn} = 0.001$ and $\text{Kn} = 0.100$ ($u_w = 0.42$; $T_w = 1.0$, $\delta t = 0.0001$). The results were obtained using the model $\text{SLB}(6;8,8,13)$ with the Shakhov collision term.

conditions when the channel walls are perpendicular to the z axis. Since the models $\text{SLB}(N; K = N + 1, L = N + 1, M = 2N + 1)$ produce more accurate results when N increases, while models $\text{SLB}(N; 8, 8, 15)$ produce results that are almost independent of N (Figs. 17 and 18), it is clear that the effect of the quadrature orders K and L on the accuracy of the Couette flow simulation results is more important than the effect of N . According to Figs. 17 and 18, the values of K and L should be at least equal to 6 to approach the DSMC results at $\text{Kn} = 0.1$.

To separate the effect of N from the effect of the boundary conditions on the accuracy of the results, as well as to check

if models of quadrature orders $K = L = 8$ are convenient for simulations at the Navier-Stokes-Fourier level ($\text{Kn} \leq 0.1$), we conducted a second series of Couette flow simulations using models $\text{SLB}(N; 8, 8, 15)$ and $\text{SLB}(N; 20, 20, 17)$, for $\text{Kn} = 0.001$ and $\text{Kn} = 0.100$ ($u_w = 0.42$; $T_w = 1.0$, $\delta s = 1/100$, $\delta t = 10^{-4}$). Both collision terms (Shakhov and BGK) were considered in these simulations. After reaching the stationary state, the temperature values T_N in a lattice node situated in the central region of the channel ($z = 0.005$) were collected in Tables II and III for $2 \leq N \leq N_{\text{max}}$, where N_{max} has the values 7 and 8, respectively (the Shakhov case with

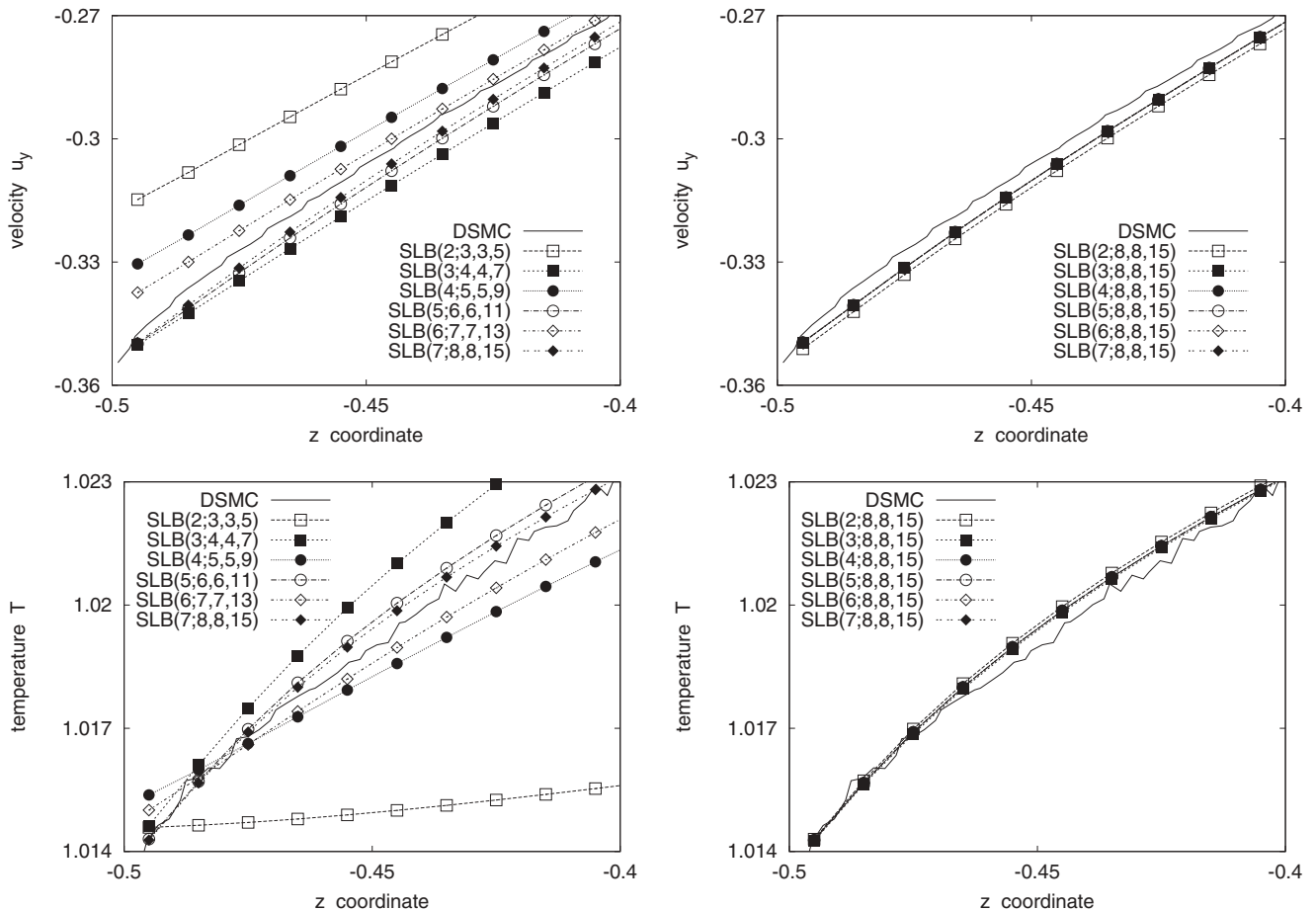


FIG. 17. Stationary profiles of velocity and temperature near the left wall in Couette flow at $\text{Kn} = 0.100$ ($u_w = 0.42$; $T_w = 1.0$), obtained with models $\text{SLB}(N; N + 1, N + 1, 2N + 1)$ and $\text{SLB}(N; 8, 8, 15)$ using the Shakhov collision term ($N = 2, \dots, 7$).

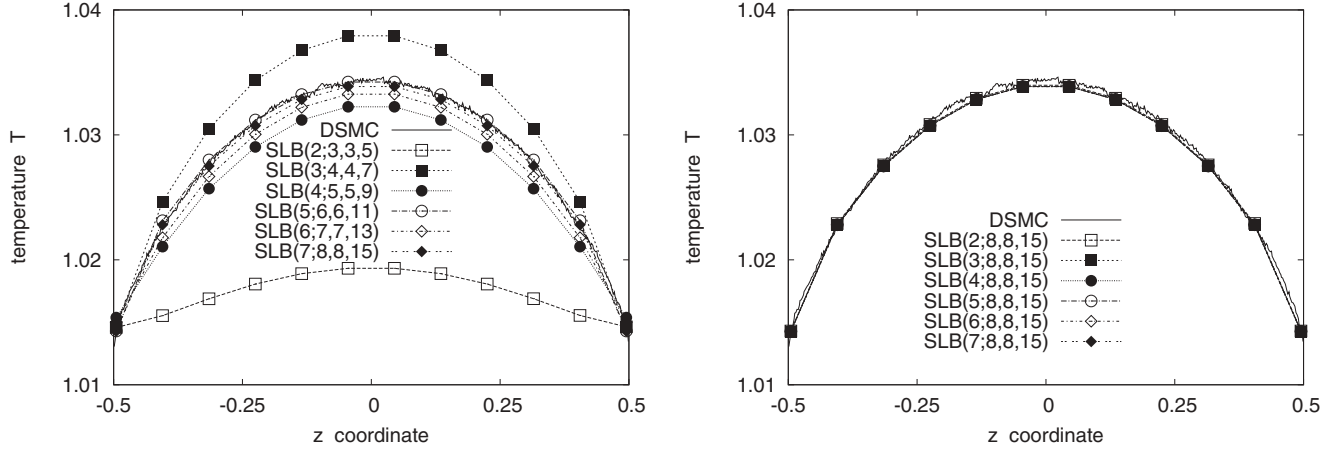


FIG. 18. Stationary profiles of temperature across the channel in Couette flow at $Kn = 0.100$ ($u_w = 0.42$; $T_w = 1.0$), obtained with models $SLB(N; N + 1, N + 1, 2N + 1)$ and $SLB(N; 8, 8, 15)$ using the Shakhov collision term ($N = 2, \dots, 7$).

$N = 2$, $Kn = 0.001$ is not present in these tables because our simulations returned nonarithmetic values).

Tables II and III show that the value for the temperature in a central node gets corrections as N is increased. When using the model $SLB(N; 8, 8, 15)$ with the BGK collision term for $Kn = 0.001$, the first eight significant figures of the temperature value stay the same for all $N \geq 4$. This confirms that the Navier-Stokes level is accurately recovered with $N_{min}^{BGK} = 4$. For the Shakhov case, $N = 4$ gives only six figures, $N = 5$ gives seven figures and $N = 6, 7$ seem to give eight significant figures that are identical. At $Kn = 0.1$, the $SLB(N; 8, 8, 15)$ model with the BGK collision term shows that seven significant figures are accurate when $N = 4, 5$, but increasing N to 6 ensures convergence up to ten significant figures. With the Shakhov model, $N = 4$ gives six significant figures, $N = 5$ raises this number to seven while $N > 5$ give up to ten significant figures that are identical.

The $SLB(N; 20, 20, 17)$ models (Table III) give similar results for the BGK case: $N_{min}^{BGK} = 4$ seems to be the minimum value of N for which seven and eight significant figures are recovered at $Kn = 0.001$ and 0.1 , respectively. The corresponding SLB models implementing the Shakhov collision term with $N \geq N_{min}^S = 5$ are accurate to eight significant figures at both $Kn = 0.001$ and $Kn = 0.1$. Increasing N to 6 ensures ten accurate digits in the temperature value at $Kn = 0.1$.

The minimum values $N_{min}^{BGK} = 4$ and $N_{min}^S = 5$, which are required for the recovery of the Navier-Stokes-Fourier level when using the BGK and the Shakhov collision terms, respectively, are also confirmed in Fig. 19. When N exceeds N_{min}^{BGK} or N_{min}^S , the relative error $T_N/T_{N_{max}} - 1$ becomes quite negligible (less than 10^{-6}) for both $SLB(N; 8, 8, 15)$ and $SLB(N; 20, 20, 17)$ results at $Kn = 0.001$ and $Kn = 0.1$. An attempt at explaining the value of N_{min}^{BGK} and N_{min}^S is made in Appendix F.

B. Finding the optimal models

For $N \geq N_{min}^S$, the peak temperature we observed in Couette flow simulations with the models $SLB(N; 20, 20, 17)$ at $Kn = 0.100$ using the Shakhov collision term when $u_w = 0.42$ and $T_w = 1.0$ exceeds the wall temperature by an amount approximately equal to the reference value $\Delta T_{ref} = 0.033814$ (Table III). We shall look for the *optimal* SLB model defined as the model which has the smallest momentum vector set and is able to retrieve the peak temperature value in Couette flow with a relative error below 1% with respect to ΔT_{ref} (i.e., $0.033476 \leq \Delta T \leq 0.034152$).

Since the occurrence of momentum vectors parallel to the bounding walls is undesirable in the SLB models, the offset angle ϕ in Eq. (18) is set to π/M , M is restricted to multiples of 4 and only even values are allowed for L . This way, there

TABLE II. Temperature values in a lattice node belonging to the central region of the Couette channel ($z = 0.005$), computed with models $SLB(N; 8, 8, 15)$ at $Kn = 0.001$ and $Kn = 0.100$ ($T_w = 1.0$, $u_w = 0.42$, $\delta_s = 0.01$, $\delta t = 10^{-4}$).

N	Shakhov		BGK	
	Kn = 0.001	Kn = 0.100	Kn = 0.001	Kn = 0.100
2	–	1.034099184002857	1.035414171136828	1.041406268511928
3	1.024191980104776	1.033988314149106	1.035405198720537	1.041405158492003
4	1.024185044160306	1.033998502667994	1.035405932242372	1.041415561165884
5	1.024183651339326	1.033997349131699	1.035405940327726	1.041415560121376
6	1.024183756789055	1.033997467946009	1.035405954841901	1.041415681094108
7	1.024183777145866	1.033997467075263	1.035405964436171	1.041415681652265

TABLE III. Temperature values in a lattice node belonging to the central region of the Couette channel ($z = 0.005$), computed with models SLB($N; 20, 20, 17$) at $\text{Kn} = 0.001$ and $\text{Kn} = 0.100$ ($T_w = 1.0$, $u_w = 0.42$, $\delta s = 0.01$, $\delta t = 10^{-4}$).

N	Shakhov		BGK	
	$\text{Kn} = 0.001$	$\text{Kn} = 0.100$	$\text{Kn} = 0.001$	$\text{Kn} = 0.100$
2	–	1.033917770404391	1.035218899719038	1.041153825468452
3	1.024077364289831	1.033813987161310	1.035206867784424	1.041153543029809
4	1.024069792328900	1.033815669767298	1.035207373441255	1.041155336986916
5	1.024068457600274	1.033814572445944	1.035207454543212	1.041155340608889
6	1.024068436025751	1.033814581437933	1.035207559540435	1.041155350240522
7	1.024068436842635	1.033814581336912	1.035207467876605	1.041155349882998
8	1.024068453774640	1.033814581273103	1.035207475994389	1.041155349717404

are no momentum vectors parallel to any plane wall as long as the walls are perpendicular to the coordinate axes.

In Table IV we show the Couette flow results when the walls are perpendicular to the z or x axis (setting the wall perpendicular to the y axis would give similar results to the x case). According to this table, the model SLB(5; 8, 6, 12) fulfills the requirements for the optimal model for geometries which include walls perpendicular to any of the coordinate axes. Actually, in Table IV one can see that all models SLB($N; 8, 6, 12$), where the value of N can be chosen as low as $N = 2$, do not exceed the upper limit of the relative error we chose for the optimal model. Alternatively, the models SLB($N; 6, 6, 12$), $2 \leq N \leq 6$, which have a smaller momentum set, might be appropriate when the error related to the temperature peak is relaxed up to approximately 2%.

VIII. CONCLUSION

In this paper we have introduced a hierarchy of spherical Lattice Boltzmann models, denoted SLB($N; K, L, M$), which ensure the recovery of all moments of the equilibrium distribution function up to order N and can be used to solve the three-dimensional Boltzmann equation numerically. Unlike current LB models that rely on the Cartesian coordinate system and the Gauss-Hermite quadrature, we used the spherical coordinate system, as well as the Gauss-Legendre and

Gauss-Laguerre quadrature formulas [105–107] to accomplish the discretization of the momentum space. The tips of the $K \times L \times M$ momentum vectors of the model SLB($N; K, L, M$) are situated on the circles defined by the intersection between K spherical shells and L parallel planes. Each circle contains M equidistant points, as shown in Fig. 1.

The characteristics of the SLB models were investigated by computer simulation of the Couette flow between parallel plates perpendicular to the z axis. To achieve the right value of the Prandtl number for the ideal gas ($\text{Pr} = 2/3$), we considered the Shakhov collision term [96–99] besides the widely used BGK term that features the unrealistic value $\text{Pr} = 1$. A flux limiter scheme was used to evolve the distribution functions in each lattice node and diffuse reflection boundary conditions were implemented on the channel walls.

The SLB simulation results obtained with the Shakhov collision term were compared to DSMC results [85–88] for various values of the Knudsen number Kn . As observed during the preliminary investigations (Figs. 4 through 6), the longitudinal velocity profiles $u_y(z)$, as well as the transversal and longitudinal heat flux profiles $q_z(z)$ and $q_y(z)$ are very close to the corresponding DSMC profiles and specific effects in microfluidics (the slip velocity, the temperature jump, as well as the longitudinal heat flux) are well captured up to $\text{Kn} = 0.50$ (Fig. 13). The temperature profiles $T(z)$ are more sensitive

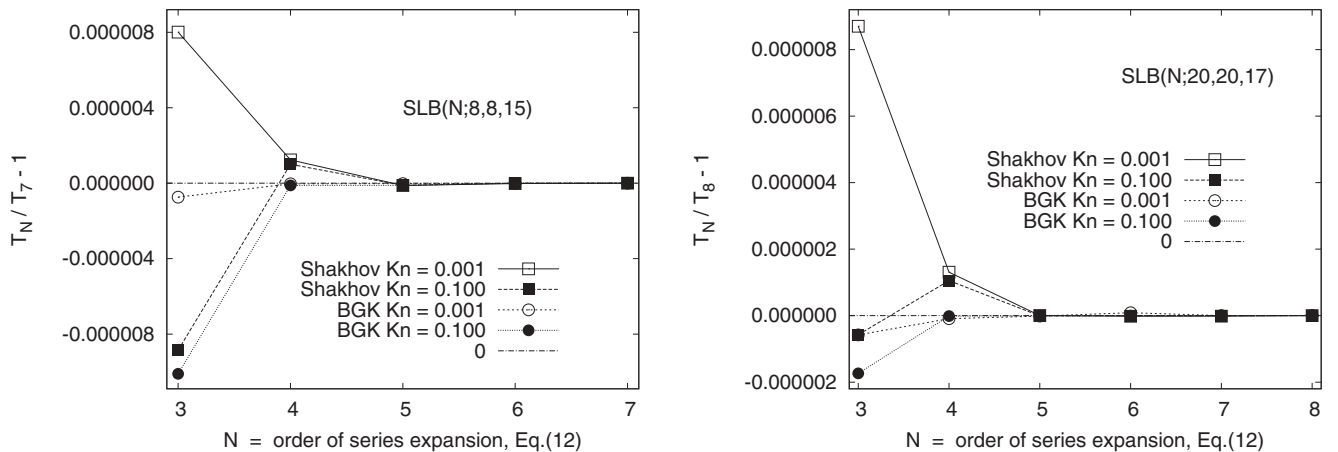


FIG. 19. Effect of series expansion N on the relative error of Couette flow results obtained with models SLB($N; 8, 8, 15$) and SLB($N; 20, 20, 17$) at $\text{Kn} = 0.001$ and $\text{Kn} = 0.100$. T_N is the fluid temperature in node $z = 0.005$ of the lattice ($u_w = 0.42$; $T_w = 1.0$; $\delta s = 0.01$; $\delta t = 10^{-4}$).

TABLE IV. Temperature values in a lattice node belonging to the central region of the Couette channel ($z = 0.005$), computed with models SLB($N; K, L, 12$) at $\text{Kn} = 0.100$ using the Shakhov collision term ($N = 2, \dots, 5$, $K, L \in \{6, 8\}$, $T_w = 1.0$, $u_w = 0.42$, $\delta s = 0.01$, $\delta t = 10^{-4}$).

SLB model	Channel walls $\perp z$ axis	Channel walls $\perp x$ axis
SLB(5; 6, 6, 12)	1.034353143000633	1.034371330774369
SLB(5; 6, 8, 12)	1.034277528046599	1.034384224321768
SLB(5; 8, 6, 12)	1.034071909199458	1.034089477729780
SLB(5; 8, 8, 12)	1.033997333345718	1.034102718864193
SLB(4; 6, 6, 12)	1.034354417336353	1.034372606941889
SLB(4; 6, 8, 12)	1.034278622687030	1.034385556462679
SLB(4; 8, 6, 12)	1.034073260081271	1.034090866008742
SLB(4; 8, 8, 12)	1.033998494366201	1.034104125256837
SLB(3; 6, 6, 12)	1.034340396079116	1.034353953406585
SLB(3; 6, 8, 12)	1.034278749044194	1.034367061985098
SLB(3; 8, 6, 12)	1.034048626623691	1.034061702865505
SLB(3; 8, 8, 12)	1.033988279334024	1.034075083772691
SLB(2; 6, 6, 12)	1.034290145222360	1.034309974340356
SLB(2; 6, 8, 12)	1.034230337741884	1.034322854462495
SLB(2; 8, 6, 12)	1.034015567947804	1.034034469222146
SLB(2; 8, 8, 12)	1.033955317278828	1.034047468762622

to changes in the quadrature orders K and L , especially for $\text{Kn} > 0.1$.

The simulation results become more accurate and a convergence process was observed when K and L are increased (Sec. VIB). The convergent behavior is due to the inaccurate recovery of the half-space integrals involved in the implementation of the diffuse reflection boundary conditions (Sec. V and Appendix E). As observed in the literature [29, 71, 101, 102, 120, 121], these integrals are more accurately recovered when the LB model does not contain any momentum vectors parallel to the channel walls. According to our Couette flow simulations at $\text{Kn} = 0.5$, the values of K and L need to be as high as 22 while at $\text{Kn} = 0.1$ the convergence is essentially achieved for $K = L = 8$.

We have confirmed both numerically (Sec. VII) and analytically (Appendix F) that the minimum order N of a SLB model that ensures the retrieval of mass, momentum, and energy equations at the Navier-Stokes-Fourier level ($\text{Kn} < 0.1$) is 4 or 5, depending on the collision term (BGK or Shakhov) used within the model. However, smaller values for the order N of the series expansion (34) seem to affect the accuracy of the results in a negligible manner since the Couette flow simulations performed with models SLB($N; 8, 6, 12$) of order N as low as $N = 2$ were found to fit the peak temperature in Couette flow with a relative error of less than 1%.

There are two main steps in the development of the SLB models: *a*, the separation of variables and *b*, the use of Gauss quadrature formulas. The resulted momentum vectors are no longer related to the lattice geometry and therefore more elaborate schemes (e.g., finite difference or flux limiter schemes) need to be used instead of the collision and streaming scheme encountered in the standard LB models. The implementation of the boundary conditions on plane walls is based on the evaluation of incoming and

outgoing fluxes, which involves half-space integration. The half-space integration (or the integration over a hemisphere that results after the radial coordinate has been separated) is a source of numerical errors that can be reduced by rejecting the SLB models containing momentum vectors parallel to the walls, as well as by increasing the order of the angular quadratures (a process that raises the computational costs). The problem of the half-space integration, which is encountered also in connection to LB models involving the Gauss-Hermite quadrature, remains a challenge for the future.

Although our SLB models were developed in the three-dimensional space, two-dimensional models based on concentric circles can be considered as well. Such models involving a circular quadrature followed by a radial one might generalize the D2Q7 LB models developed two decades ago on a triangular lattice [3, 13–15, 89, 94], as well as the 2D model originally developed by Watari and Tsutahara [31, 32, 103]. The use of SLB models to investigate various problems related to transport phenomena in single or multicomponent fluids with one or more phases present, as well as the comparison of SLB models to LB models based on the Gauss-Hermite quadrature require future work.

ACKNOWLEDGMENTS

This work was supported by CNCSIS-UEFISCSU Project No. PNII-IDEI code ID_76/2010. The computer simulations reported in this paper were done using the Portable Extensible Toolkit for Scientific Computation (PETSc 3.1) developed at Argonne National Laboratory, Argonne, Illinois [125]. We thank our collaborators and friends Professor Daniel Vizman (Department of Physics, West University of Timișoara, Romania), Professor Giuseppe Gonnella (Department of Physics, University of Bari, Italy) and Doctor Antonio Lamura (Institute for the Applications of Calculus “Mauro Picone,” CNR, Section of Bari, Italy) for encouragement, as well as for sharing with us the CPU time available on the NANOSIM cluster (Department of Physics, West University of Timișoara, Romania), IBM SP6 system (CINECA, Casalecchio di Reno, Bologna, Italy, INFN convention) and MATRIX cluster (CASPUR, Rome, Italy, Standard HPC Grant 2010/2011). Access to the IBM Blue Gene/P supercomputer managed by Professor Dana Petcu, Silviu Panica, and Marian Neagul at the West University of Timișoara is also acknowledged. The authors express their gratitude to Professor Henning Struchtrup (Department of Mechanical Engineering, University of Victoria, Canada) for kindly providing the DSMC simulation results used to validate the SLB models introduced in this paper. V.S. remains very grateful to Professor Michihisa Tsutahara (Department of Mechanical Engineering, Kobe University, Japan), as well as to Professor Minoru Watari (LBM Fluid Dynamics Laboratory, Gifu, Japan) for careful hospitality and fruitful discussions started during his visits to Kobe (2007 and 2008).

APPENDIX A: GAUSS QUADRATURES

Gaussian quadratures are quadrature methods which exactly recover integrals of the form

$$\int_{\mathcal{D}} dx w(x)g(x),$$

where \mathcal{D} is the integration domain, $g(x)$ is a polynomial in x , and $w(x)$ is a suitable weight function such that there exists a complete set of orthogonal polynomials $\phi_n(x)$ satisfying the orthogonality relation

$$\int_{\mathcal{D}} dx w(x)\phi_n(x)\phi_m(x) = \gamma_n \delta_{nm}. \quad (\text{A1})$$

The integer subscripts n, m indicate the order of the polynomials, the Kronecker delta symbol δ_{nm} takes the value 1 when $n = m$ and 0 otherwise, and γ_n is a constant which depends on the set of polynomials $\{\phi_n\}$.

For the recovery of integrals of polynomials of order less than or equal to Q , a Gaussian quadrature method employs a number of m quadrature points x_k ($k = 1, 2, \dots, m$) such that $2m > Q$

$$\int_{\mathcal{D}} dx w(x)g(x) = \sum_{k=1}^m w_k g(x_k). \quad (\text{A2})$$

The weights w_k in Eq. (A2) can be computed using the formula

$$w_k = \int_{\mathcal{D}} dx w(x) \frac{\Phi_m(x)}{(x - x_k)\Phi'_m(x_k)}. \quad (\text{A3})$$

Based on general properties of sets of orthogonal polynomials [107], Eq. (A3) can be simplified to

$$w_k = -\frac{A_{m+1}\gamma_m}{A_m\Phi_{m+1}(x_k)\Phi'_m(x_k)}, \quad (\text{A4})$$

where A_m is the coefficient of the highest power of x in $\Phi_m(x)$ and γ_m is defined by Eq. (A1).

APPENDIX B: LEGENDRE POLYNOMIALS

The Legendre polynomials [106,107] form a complete set of solutions to Legendre's equation

$$\left[(1 - z^2) \frac{d^2}{dz^2} - 2z \frac{d}{dz} + \ell(\ell + 1) \right] P_\ell(z) = 0, \quad (\text{B1})$$

and have the following polynomial form:

$$P_\ell(z) = \frac{1}{2^\ell} \sum_{i=0}^{\lfloor \ell/2 \rfloor} (-1)^i z^{\ell-2i} \binom{2\ell-2i}{\ell} \binom{\ell}{i}, \quad (\text{B2})$$

where the binomial coefficient is defined as [106]

$$\binom{n}{k} = \frac{n!}{k!(n-k)!}. \quad (\text{B3})$$

The coefficient of the highest power in the Legendre polynomial of order ℓ is

$$A_\ell = \frac{(2\ell)!}{2^\ell(\ell!)^2}. \quad (\text{B4})$$

The Legendre polynomials are orthogonal on the domain $\mathcal{D} = [-1, 1]$

$$\int_{-1}^1 dz P_\ell(z)P_{\ell'}(z) = \frac{2}{2\ell+1} \delta_{\ell\ell'}, \quad (\text{B5})$$

which sets

$$\gamma_\ell = \frac{2}{2\ell+1}. \quad (\text{B6})$$

The following recursion formula can be used for the automatic computation of higher-order polynomials

$$(\ell+1)P_{\ell+1}(z) = (2\ell+1)zP_\ell(z) - \ell P_{\ell-1}(z). \quad (\text{B7})$$

The first few members of the set are

$$\begin{aligned} P_0(z) &= 1, & P_1(z) &= z, \\ P_2(z) &= \frac{3}{2}z^2 - \frac{1}{2}, & P_3(z) &= \frac{5}{2}z^3 - \frac{3}{2}z, \\ P_4(z) &= \frac{35}{8}z^4 - \frac{15}{4}z^2 + \frac{3}{8}, \\ P_5(z) &= \frac{63}{8}z^5 - \frac{35}{4}z^3 + \frac{15}{8}z. \end{aligned}$$

The set of Legendre polynomials $P_\ell(z)$ is used in the Gauss-Legendre quadrature method for the exact integration of polynomials on the domain $\mathcal{D} = [-1, 1]$ with weight function $w(z) = w^{(P)}(z) \equiv 1$. Integrals of polynomials of order less than or equal to Q can be recovered by using L quadrature points, as long as $2L > Q$. The corresponding weights $w_j^{(P)}$, $j = 1, 2, \dots, L$, defined as w_j in Eq. (A2), can be evaluated using the formula

$$w_j^{(P)} = \frac{2(1 - z_j^2)}{(L+1)^2 [P_{L+1}(z_j)]^2}, \quad (\text{B8})$$

TABLE V. The roots z_j ($j = 1, 2, \dots, L$) of the Legendre polynomials $P_L(z)$, $L = 1, 2, \dots, 8$, and their corresponding weights $w_j^{(P)}$.

L	z_j	$w_j^{(P)}$
1	0	2
2	± 0.5773502691896258	1
3	0	0.8888888888888889
	± 0.7745966692414834	0.5555555555555556
4	± 0.3399810435848563	0.6521451548625461
	± 0.8611363115940526	0.3478548451374539
5	0	0.5688888888888889
	± 0.5384693101056831	0.4786286704993665
	± 0.9061798459386640	0.2369268850561891
6	± 0.2386191860831969	0.4679139345726910
	± 0.6612093864662645	0.3607615730481386
	± 0.9324695142031520	0.1713244923791703
7	0	0.4179591836734694
	± 0.4058451513773972	0.3818300505051189
	± 0.7415311855993944	0.2797053914892767
	± 0.9491079123427585	0.1294849661688697
8	± 0.1834346424956498	0.3626837833783620
	± 0.5255324099163290	0.3137066458778873
	± 0.7966664774136267	0.2223810344533745
	± 0.9602898564975362	0.1012285362903762

which follows from Eq. (A4) using the results (B4) and (B6), as well as the formula for the derivative of P_ℓ

$$\frac{1 - z^2}{\ell + 1} \frac{d}{dz} P_\ell(z) = -P_{\ell+1}(z) + zP_\ell(z). \quad (B9)$$

The points z_j are the roots of the Legendre polynomial of order L [i.e., $P_L(z_j) = 0$]. A list of the roots z_j ($j = 1, 2, \dots, L$) of the Legendre polynomials of order $L = 2, 3, \dots, 9$ and their corresponding weights $w_j^{(P)}$ is given in Table V.

APPENDIX C: LAGUERRE POLYNOMIALS

The generalized Laguerre polynomials $L_k^{(\alpha)}(x)$ form a complete set of solutions to the generalized Laguerre equation [106,107]

$$\left[x \frac{d^2}{dx^2} + (\alpha + 1 - x) \frac{d}{dx} + k \right] L_k^{(\alpha)}(x) = 0, \quad (C1)$$

and have the following polynomial form:

$$L_k^{(\alpha)}(x) = \sum_{s=0}^k \frac{\Gamma(\alpha + k + 1)}{\Gamma(\alpha + s + 1)} \frac{(-x)^s}{s!(k - s)!}. \quad (C2)$$

Here, $\alpha > -1$ is a real number and

$$\Gamma(\nu + 1) = \int_0^\infty dx x^\nu e^{-x} \quad (C3)$$

is the Gamma (factorial) function [106], which satisfies the recurrence relation $\Gamma(\nu + 1) = \nu\Gamma(\nu)$ and reduces to $\Gamma(k + 1) = k!$ when $k \geq 0$ is an integer number. The coefficient A_k of the highest power of x in $L_k^{(\alpha)}$ is readily determined from Eq. (C2)

$$A_k = \frac{(-1)^k}{k!}. \quad (C4)$$

The generalized Laguerre polynomials satisfy the orthogonality relation

$$\int_0^\infty dx w^{(L)}(x) L_k^{(\alpha)}(x) L_{k'}^{(\alpha)}(x) = \frac{\Gamma(k + \alpha + 1)}{\Gamma(k + 1)} \delta_{kk'} \quad (C5)$$

on the domain $\mathcal{D} = [0, \infty)$, with respect to the weight function

$$w^{(L)}(x) = x^\alpha e^{-x}, \quad (C6)$$

which sets the value of γ_k to

$$\gamma_k = \frac{\Gamma(k + \alpha + 1)}{\Gamma(k + 1)}. \quad (C7)$$

The first few members of the family of generalized Laguerre polynomials $L_\ell^{(\alpha)}(x)$ are given below:

$$\begin{aligned} L_0^{(\alpha)}(x) &= 1, & L_1^{(\alpha)}(x) &= -x + \alpha + 1, \\ L_2^{(\alpha)}(x) &= \frac{1}{2!}x^2 - (\alpha + 2)x + \frac{1}{2!}(\alpha + 1)(\alpha + 2), \\ L_3^{(\alpha)}(x) &= -\frac{1}{3!}x^3 + \frac{1}{2!}(\alpha + 3)x^2 \\ &\quad - \frac{1}{2!}(\alpha + 2)(\alpha + 3)x + \frac{1}{3!}(\alpha + 1)(\alpha + 2)(\alpha + 3), \\ L_4^{(\alpha)}(x) &= \frac{1}{4!}x^4 - \frac{1}{3!}(\alpha + 4)x^3 \end{aligned}$$

TABLE VI. Roots x_k and weights $w_k^{(L)}$, $k = 1, 2, \dots, K$, for the generalized Laguerre polynomials $L_K^{(1/2)}(x)$, $K = 2, 3, \dots, 9$.

K	x_k	$w_k^{(L)}$
2	0.9188611699158103	0.7233630235462755
	4.081138830084190	0.1628639019064826
3	0.6663259077023708	0.5671862778403113
	2.800775054150257	0.3053717688445466
	7.032899038147373	$1.366887876790013 \times 10^{-2}$
	0.5235260767382691	0.4530087465586076
4	2.156648763269094	0.3816169601717997
	5.137387546176712	$5.079462757224076 \times 10^{-2}$
	10.18243761381592	$8.065911501100308 \times 10^{-4}$
	0.4313988071478515	0.3704505700074585
5	1.759753698423696	0.4125843737694529
	4.104465362828315	$9.777982005318071 \times 10^{-2}$
	7.746703779542557	$5.373415341171987 \times 10^{-3}$
	13.45767835205758	$3.874628149393572 \times 10^{-5}$
	0.3669498773083707	0.3094240968362601
6	1.488534292310452	0.4177521497070222
	3.434007968424071	0.1432858732209769
	6.349067925680380	$1.533249102263384 \times 10^{-2}$
	10.54046985844834	$4.306911960439409 \times 10^{-4}$
	16.82097007782838	$1.623469821074071 \times 10^{-6}$
	0.3193036339206301	0.2631245143958920
	1.290758622959153	0.4091418694141023
7	2.958374458696650	0.1821177320927161
	5.409031597244433	$3.005332430127097 \times 10^{-2}$
	8.804079578056775	$1.760894117540062 \times 10^{-3}$
	13.46853574325148	$2.852947122115973 \times 10^{-5}$
	20.24991636587088	$6.166001541039145 \times 10^{-8}$
	0.2826336481165991	0.2271393619524716
8	1.139873801581614	0.3935945428036153
	2.601524843406029	0.2129089708672281
	4.724114537527791	$4.787748320313819 \times 10^{-2}$
	7.605256299231614	$4.542517474762636 \times 10^{-3}$
	11.41718207654583	$1.624046001853259 \times 10^{-4}$
	16.49941079765582	$1.642377413806098 \times 10^{-6}$
	23.73000399593471	$2.173943126630918 \times 10^{-9}$
	0.2535325549744191	0.1985712548680195
9	1.020844277720390	0.3749207846631710
	2.323096077022466	0.2360748210008250
	4.199350600657293	$6.709610500320429 \times 10^{-2}$
	6.713974316615029	$9.008508896644318 \times 10^{-3}$
	9.972009159539349	$5.426607386359321 \times 10^{-4}$
	14.15405367127805	$1.270536687910836 \times 10^{-5}$
	19.61190281916595	$8.484309239668555 \times 10^{-8}$
27.25123652302706	$7.228647164396524 \times 10^{-11}$	

$$\begin{aligned} &+ \frac{1}{2!2!}(\alpha + 3)(\alpha + 4)x^2 - \frac{1}{3!}(\alpha + 2) \cdots (\alpha + 4)x \\ &+ \frac{1}{4!}(\alpha + 1) \cdots (\alpha + 4), \\ L_5^{(\alpha)}(x) &= -\frac{1}{5!}x^5 + \frac{1}{4!}(\alpha + 5)x^4 \\ &- \frac{1}{3!2!}(\alpha + 4)(\alpha + 5)x^3 + \frac{1}{2!3!}(\alpha + 3) \cdots (\alpha + 5)x^2 \\ &- \frac{1}{4!}(\alpha + 2) \cdots (\alpha + 5)x + \frac{1}{5!}(\alpha + 1) \cdots (\alpha + 5). \end{aligned}$$

The following recursion formula can be used for the automatic computation of higher-order Laguerre polynomials:

$$kL_k^{(\alpha)}(x) = (2k - 1 + \alpha - x)L_{k-1}^{(\alpha)}(x) - (\alpha + k - 1)L_{k-2}^{(\alpha)}(x). \quad (\text{C8})$$

The Laguerre polynomials are used in the Gauss-Laguerre quadrature method, which allows the exact recovery of integrals of polynomials over the domain $[0, \infty)$ with respect to the weight function (C6). For the exact recovery of integrals of polynomials of order Q , the number K of quadrature points must satisfy $2K > Q$. An example of the application of this quadrature rule is given in Sec. II B, where $Q = 2N$, with the lower bounds on the quadrature orders given in Eq. (35).

The discrete weights [defined by Eq. (A3)] can be evaluated using the formula

$$w_k^{(L)} = \frac{x_k \Gamma(K + 1 + 1/2)}{K!(K + 1)^2 [L_{K+1}^{(1/2)}(x_k)]^2}. \quad (\text{C9})$$

The points x_k are the roots of the K th order polynomial [i.e., $L_K^{(1/2)}(x_k) = 0, k = 1, \dots, K$]. Equation (C9) can be obtained from Eq. (A4) using Eqs. (C4) and (C7), as well as the property

$$x \frac{dL_k^{(\alpha)}(x)}{dx} = (k + 1)L_{k+1}^{(\alpha)}(x) - (\alpha + k + 1 - x)L_k^{(\alpha)}(x). \quad (\text{C10})$$

The roots and corresponding weights for $K = 2, \dots, 9$ are listed in Table VI.

APPENDIX D: HERMITE POLYNOMIALS

In this section we present some of the general features of the Hermite polynomials in an arbitrary number of dimensions, selected from [18,126]. In what follows, Greek indices go from 1 to the number of dimensions D and the Hermite polynomial of order n is a totally symmetric tensor with n indices and components $\mathcal{H}_{\alpha_1, \alpha_2, \dots, \alpha_n}^{(n)}(\mathbf{x})$, and $\mathbf{x} = (x_1, x_2, \dots, x_D)$ is a D -dimensional vector. The first members of the set have the following expressions:

$$\mathcal{H}^{(0)}(\mathbf{x}) = 1, \quad (\text{D1a})$$

$$\mathcal{H}_{\alpha}^{(1)}(\mathbf{x}) = x_{\alpha}, \quad (\text{D1b})$$

$$\mathcal{H}_{\alpha\beta}^{(2)}(\mathbf{x}) = x_{\alpha}x_{\beta} - \delta_{\alpha\beta}, \quad (\text{D1c})$$

$$\mathcal{H}_{\alpha\beta\gamma}^{(3)}(\mathbf{x}) = x_{\alpha}x_{\beta}x_{\gamma} - (x_{\alpha}\delta_{\beta\gamma} + x_{\beta}\delta_{\alpha\gamma} + x_{\gamma}\delta_{\alpha\beta}). \quad (\text{D1d})$$

Higher-order polynomials can be obtained using the recursion

$$\mathcal{H}_{\alpha_1, \dots, \alpha_n}^{(n)}(\mathbf{x}) = x_{\alpha_1} \mathcal{H}_{\alpha_2, \dots, \alpha_n}^{(n-1)}(\mathbf{x}) - [\delta_{\alpha_1 \alpha_2} \mathcal{H}_{\alpha_3, \dots, \alpha_n}^{(n-2)} + \delta_{\alpha_1 \alpha_3} \mathcal{H}_{\alpha_2, \alpha_4, \dots, \alpha_n}^{(n-2)} \dots + \delta_{\alpha_1 \alpha_n} \mathcal{H}_{\alpha_2, \dots, \alpha_{n-1}}^{(n-2)}]. \quad (\text{D2})$$

The Hermite polynomials are orthogonal over the domain $\mathcal{D} = \mathbb{R}^D$ with respect to the weight function $e^{-x^2/2}$

$$\int \frac{d^D x}{(2\pi)^{D/2}} e^{-x^2/2} \mathcal{H}_{\alpha_1, \dots, \alpha_m}^{(m)}(\mathbf{x}) \mathcal{H}_{\beta_1, \dots, \beta_n}^{(n)}(\mathbf{x}) = \delta_{nm} \sum_{\sigma \in S_n} \prod_{i=1}^n \delta_{\alpha_i \beta_{\sigma_i}}. \quad (\text{D3})$$

Here S_n is the set of $n!$ permutations of $1, 2, \dots, n$, for example,

$$\int \frac{d^D x}{(2\pi)^{D/2}} e^{-x^2/2} \mathcal{H}_{\alpha\beta}^{(2)}(\mathbf{x}) \mathcal{H}_{\mu\nu}^{(2)}(\mathbf{x}) = \delta_{\alpha\mu} \delta_{\beta\nu} + \delta_{\alpha\nu} \delta_{\beta\mu} \quad (\text{D4})$$

and for $n = 3$ the set of all permutations is $S_3 = \{1, 2, 3\}, \{2, 3, 1\}, \{3, 1, 2\}, \{1, 3, 2\}, \{3, 2, 1\}, \{2, 1, 3\}$.

APPENDIX E: IMPACT OF DIFFUSE REFLECTION BOUNDARY CONDITIONS ON SLB RESULTS FOR COUETTE FLOW

The diffuse reflection boundary conditions can be phrased as

$$f(\mathbf{x}_w, \mathbf{p}, t) = f_w^{(0)}(\mathbf{x}_w, \mathbf{p}, t), \quad (\mathbf{p} \cdot \mathbf{n} < 0), \quad (\text{E1a})$$

where \mathbf{n} is the outwards normal of the bounding surface at point \mathbf{x}_w , D is the number of dimensions, f is the distribution function, and $f^{(0)}$ is the equilibrium distribution function. The equilibrium distribution function $f_w^{(0)}$ is fully determined by the value of the wall temperature T_w and velocity u_w , which are fixed by boundary conditions, and the density n_w , implicitly given by

$$\int_{p_n > 0} d^D p f p_n = - \int_{p_n < 0} d^D p f_w^{(0)} p_n. \quad (\text{E1b})$$

Here $p_n = \mathbf{p} \cdot \mathbf{n}$ is the projection of the momentum \mathbf{p} on the outwards normal \mathbf{n} .

To illustrate, let us consider the problem of Couette flow between the parallel plates investigated in Sec. VI. The plates are perpendicular to the z axis while the flow is along the y axis. On the upper wall, Eq. (E1b) takes the form

$$\int_{p_z > 0} d^3 p f p_z = \int_{p_z < 0} d^3 p f_w^{(0)} p_z. \quad (\text{E2})$$

In the stationary state the only nonvanishing component of the fluid velocity is u_y , in which case $p_z = \xi_z$. For simplicity, let $f^{(0)}$ be the Maxwellian given by Eq. (4). The integral of the equilibrium distribution function can be performed in the Cartesian coordinate system and yields

$$\int_{p_z < 0} d^3 p f_w^{(0)} p_z = -n_w \sqrt{\frac{m T_w}{2\pi}}, \quad (\text{E3})$$

which proves that Eq. (E1b) fixes n_w . The left-hand side of Eq. (E2) can be analyzed qualitatively as follows. Since the flow has translational symmetry along the x and y axes, the derivatives with respect to x and y automatically vanish, therefore, the Boltzmann equation takes the form

$$\frac{p_z}{m} \partial_z f = -\frac{1}{\tau} (f - f^{(0)}). \quad (\text{E4})$$

The Chapman-Enskog solution to this equation is

$$f = \sum_{j=0}^{\infty} f^{(j)}, \quad f^{(j)} = \left(-\frac{\tau p_z}{m} \partial_z\right)^j f^{(0)}. \quad (\text{E5})$$

Thus, the evaluation of the integral in the left-hand side of Eq. (E2) reduces to the evaluation of integrals of the form

$$\int_{p_z > 0} d^3 p f^{(0)}(\mathbf{p}, \mathbf{x}_w, t) p_z^{j+1}. \quad (\text{E6})$$

The integral in Eq. (E6) can be calculated exactly

$$\int_{p_z > 0} d^3 p f^{(0)} p_z^{j+1} = \frac{n}{\sqrt{2\pi}} (mT)^{\frac{j+1}{2}} I_{j+1}, \quad (\text{E7})$$

where I_{j+1} is given in terms of the Gamma function (C3) by

$$I_{j+1} = \int_0^\infty dz e^{-\frac{1}{2}z^2} z^{j+1} = 2^{j/2} \Gamma\left(1 + \frac{j}{2}\right). \quad (\text{E8})$$

Using the expansion (E5) of the distribution function, the integral in Eq. (E2) can be expressed as a series in powers of the relaxation time τ

$$\begin{aligned} \int_{p_z > 0} d^3 p f p_z &= \sum_{j=0}^{\infty} \frac{\Gamma(1 + \frac{j}{2})}{\sqrt{4\pi}} \left(-\frac{\tau}{m} \partial_z\right)^j [n(2mT)^{\frac{j+1}{2}}] \\ &= n \sqrt{\frac{mT}{2\pi}} - \tau \partial_z \frac{nT}{2} + \tau^2 \partial_z^2 nT \sqrt{\frac{2T}{\pi m}} + \dots \end{aligned} \quad (\text{E9})$$

The first order in the Knudsen number vanishes since in the Couette flow the product nT is a constant, therefore, the corrections to Eq. (E3) are of order Kn^2 . This first correction requires the recovery of the integral

$$\int_{p_z > 0} d^3 p f^{(0)} p_z^3. \quad (\text{E10})$$

Integrals of odd powers of p_z over the domain $p_z > 0$ can be written as

$$\begin{aligned} \int_{p_z > 0} d^3 p f^{(0)} p_z^{2j+1} &= \frac{1}{4} \int_0^\infty x^{1/2} dx x^{j+1/2} \\ &\times \int_{-1}^1 d \cos \theta |\cos \theta|^{2j+1} \int_0^{2\pi} d\varphi f^{(0)}. \end{aligned} \quad (\text{E11})$$

The φ integral can be recovered exactly since it involves a finite-order trigonometric polynomial in $\sin \varphi$ and $\cos \varphi$ coming from the truncated polynomial expansion of $f^{(0)}$. The integral with respect to θ in Eq. (E11) above contains the term $|\cos \theta|$, which cannot be recovered using Gauss-Legendre quadrature rules. The value of such quadrature sums converges to the exact value as the number of quadrature points L is increased. In Sec. II B the quadrature method for the p integral is chosen assuming the φ and θ integrals run over the entire sphere, the exact recovery of which would prevent integrands with odd powers of p . However, in this case the Gauss-Laguerre quadrature is faced with the problem of recovering nonpolynomial terms of the form $x^{j+1/2}$. The value given by the quadrature slowly converges to the exact value as K increases.

The recovery of integrals of the form (E6) is necessary for an accurate computation of the values of the macroscopic density, velocity, and temperature near the wall, which in turn have a global influence on their corresponding profile. Equation (E9) shows that the recovery of coefficients of increasing powers of Kn require increasing values of the quadrature orders K and L .

APPENDIX F: OPTIMAL SLB MODELS

By definition, $\text{SLB}(N; K, L, M)$ is a spherical LB model which ensures the exact recovery of moments of the Maxwell-Boltzmann equilibrium distribution function of order up to and including N . In practice, it can be shown that even though the recovery of the macroscopic equations involves moments of order N' , the values of the parameters of the SLB model required for the exact recovery of the equations can be lower than the values required by Eq. (35). In this Appendix the effect of boundary conditions shall not be considered.

Let us first look at the Navier-Stokes-Fourier level of the Shakhov model. The conservation equations can be obtained from Eqs. (49) and (50). The constraints on the values of the parameters N, K, L , and M come from the equation

$$\begin{aligned} \partial_{t_1} f^{(0)} + \left(\partial_{t_0} + \frac{1}{m} p_\gamma \partial_\gamma\right) \left[f^{(0)} \mathbb{S}^{(1)} - \tau \partial_{t_0} f^{(0)} - \frac{\tau}{m} p_\gamma \partial_\gamma f^{(0)} \right] \\ = \frac{1}{\tau} f^{(0)} \mathbb{S}^{(2)} - \frac{1}{\tau} f^{(2)} \end{aligned} \quad (\text{F1})$$

with the Shakhov collision term given by Eq. (37). The highest-order moment necessary for the recovery of the energy equation comes from integrating the Shakhov term in Eq. (F1), multiplied by $p^2/2m$

$$\int d^D p f^{(0)} p^2 p_\alpha \xi^2 \xi_\beta. \quad (\text{F2})$$

At first sight, the recovery of the integral in Eq. (F2) would require $N \geq 6$, with the minimal model being $\text{SLB}(6; 7, 7, 13)$, which employs 637 roots. However, given that the Shakhov collision term contains only powers of the peculiar momentum ξ_β , the result of the integral shall be a polynomial of order 3 in the macroscopic velocity, therefore the value for N can be chosen to be smaller than 6.

Let us assume that we are employing an SLB model with $N = 5$. In this case, the angular part $E^{(5)}$ of $f^{(0)}$ defined by Eq. (11) shall be a polynomial of order 5 in p_α . The exact recovery of the angular part of the integral in Eq. (F2) requires $M \geq 12$ and $L \geq 6$ and eliminates all odd powers of p_α , leaving a polynomial of order 10 in the magnitude p of the momentum for the radial integral

$$\int_0^\infty dp p^2 F(p^2) p^{10} = \frac{1}{2} \int_0^\infty dx x^{1/2} F(x) x^5. \quad (\text{F3})$$

The recovery of the above integral requires $K \geq 6$, therefore, the minimal model capable of recovering the Navier-Stokes-Fourier level of the Shakhov model is $\text{SLB}(5; 6, 6, 12)$, which has only 432 roots.

The key assumption in the above derivation was that the recovery of the Shakhov model at NSF level requires the recovery of moments of up to order 6, but the relevant macroscopic equations contain terms of up to order 5 in the fluid velocity u_α .

Let us now look at the Navier-Stokes-Fourier level of the BGK model. The constraints on the SLB model come from Eq. (F1) with the Shakhov term set to 0

$$\partial_n f^{(0)} - \left(\partial_{t_0} \frac{1}{m} p_\gamma \partial_\gamma \right) \left[\tau \partial_{t_0} f^{(0)} + \frac{\tau}{m} p_\gamma \partial_\gamma f^{(0)} \right] = -\frac{1}{\tau} f^{(2)}. \quad (\text{F4})$$

The energy equation requires the exact recovery of the following integral:

$$\int d^D p f^{(0)} \mathbf{p}^2 p_\alpha p_\beta, \quad (\text{F5})$$

which sets the lower bound for N at 4. According to the discussion in Sec. III, the minimal model should be SLB(4; 5,5,9). However, since the square length \mathbf{p}^2 of the momentum has no angular part, the quadrature parameters on the angular part can be decreased to $L = 5, M = 8$ and as a result, the minimal model for the recovery of the NSF level of the BGK model is SLB(4; 5,5,8). The value $M = 8$ is in agreement with the 2D thermal model introduced by Watari and Tsutahara [31].

-
- [1] R. Benzi, S. Succi, and M. Vergassola, *Phys. Rep.* **222**, 145 (1992).
- [2] S. Chen and G. D. Doolen, *Annu. Rev. Fluid Mech.* **30**, 329 (1998).
- [3] S. Succi, *The Lattice Boltzmann Equation for Fluid Dynamics and Beyond* (Clarendon Press, Oxford, 2001).
- [4] M. C. Sukop and D. T. Thorne, *Lattice Boltzmann Modeling: An Introduction for Geoscientists and Engineers* (Springer, Berlin, 2006).
- [5] J. E. Broadwell, *J. Fluid Mech.* **19**, 401 (1964).
- [6] R. Gatignol, *Théorie Cinétique des Gaz à Répartition Discrète de Vitesses* (Springer, Berlin, 1975).
- [7] H. Cabannes, The Discrete Boltzmann Equation—Lecture Notes given at the University of California at Berkeley during the Spring Quarter, 1980 (unpublished). Revised version by H. Cabannes, R. Gatignol, and L. S. Luo, available at [http://henri.cabannes.free.fr/Cours_de_Berkeley.pdf].
- [8] L. S. Luo, *Comput. Phys. Commun.* **129**, 63 (2000).
- [9] G. R. McNamara and G. Zanetti, *Phys. Rev. Lett.* **61**, 2332 (1988).
- [10] F. Higuera, S. Succi, and R. Benzi, *Europhys. Lett.* **9**, 345 (1989).
- [11] F. Higuera and J. Jimenez, *Europhys. Lett.* **9**, 663 (1989).
- [12] S. Succi, R. Benzi, and F. Higuera, *Physica D* **47**, 219 (1991).
- [13] D. Rothman and S. Zaleski, *Lattice Gas Cellular Automata: Simple Models of Complex Hydrodynamics* (Cambridge University Press, Cambridge, England, 1997).
- [14] B. Chopard and M. Droz, *Cellular Automata Modeling of Physical Systems* (Cambridge University Press, Cambridge, England, 1998).
- [15] D. A. Wolf-Gladrow, *Lattice-Gas Cellular Automata and Lattice Boltzmann Models* (Springer, Berlin, 2000).
- [16] A. Scagliarini, L. Biferale, M. Sbragaglia, K. Sugiyama, and F. Toschi, *Phys. Fluids* **22**, 055101 (2010).
- [17] S. S. Chikatamarla and I. V. Karlin, *Phys. Rev. Lett.* **97**, 190601 (2006).
- [18] X. W. Shan, X. F. Yuan, and H. D. Chen, *J. Fluid Mech.* **550**, 413 (2006).
- [19] H. D. Chen, I. Goldhirsch, and S. A. Orszag, *J. Sci. Comput.* **34**, 87 (2008).
- [20] X. W. Shan, *Phys. Rev. E* **81**, 036702 (2010).
- [21] P. C. Philippi, L. A. Hegele Jr., L. O. E. dos Santos, and R. Surmas, *Phys. Rev. E* **73**, 056702 (2006).
- [22] D. N. Siebert, L. A. Hegele Jr., R. Surmas, L. O. E. dos Santos, and P. C. Philippi, *Int. J. Mod. Phys. C* **18**, 546 (2007).
- [23] D. N. Siebert, L. A. Hegele Jr., and P. C. Philippi, *Phys. Rev. E* **77**, 026707 (2008).
- [24] R. Surmas, C. E. Pico Ortiz, and P. C. Philippi, *Eur. Phys. J. Special Topics* **171**, 81 (2009).
- [25] S. S. Chikatamarla, S. Ansumali, and I. V. Karlin, *Phys. Rev. Lett.* **97**, 010201 (2006).
- [26] S. S. Chikatamarla and I. V. Karlin, *Phys. Rev. E* **79**, 046701 (2009).
- [27] M. Sbragaglia, R. Benzi, L. Biferale, S. Succi, K. Sugiyama, and F. Toschi, *Phys. Rev. E* **75**, 026702 (2007).
- [28] J. P. Meng and Y. H. Zhang, *J. Comput. Phys.* **230**, 835 (2011).
- [29] J. P. Meng and Y. H. Zhang, *Phys. Rev. E* **83**, 036704 (2011).
- [30] J. P. Meng, Y. H. Zhang, and X. W. Shan, *Phys. Rev. E* **83**, 046701 (2011).
- [31] M. Watari and M. Tsutahara, *Phys. Rev. E* **67**, 036306 (2003).
- [32] M. Watari and M. Tsutahara, *Phys. Rev. E* **70**, 016703 (2004).
- [33] M. Watari and M. Tsutahara, *Physica A* **364**, 129 (2006).
- [34] F. Nannelli and S. Succi, *J. Stat. Phys.* **68**, 401 (1992).
- [35] S. Succi, G. Amati, and R. Benzi, *J. Stat. Phys.* **81**, 5 (1995).
- [36] G. McNamara, A. L. Garcia, and B. J. Alder, *J. Stat. Phys.* **81**, 395 (1995).
- [37] M. B. Reider and J. D. Sterling, *Comput. Fluids* **24**, 459 (1995).
- [38] N. Cao, S. Chen, S. Jin, and D. Martinez, *Phys. Rev. E* **55**, R21 (1997).
- [39] R. Mei and W. Shyy, *J. Comput. Phys.* **143**, 426 (1998).
- [40] W. Shi, W. Shyy, and R. Mei, *Numer. Heat Transfer, Part B* **40**, 1 (2001).
- [41] S. Teng, Y. Chen, and H. Ohashi, *Int. J. Heat Fluid Flow* **21**, 112 (2000).
- [42] T. Seto, K. Kono, D. Martinez, and S. Chen, *JSME Int. J. Ser. B* **43**, 305 (2000).
- [43] V. Sofonea, A. Lamura, G. Gonnella, and A. Cristea, *Phys. Rev. E* **70**, 046702 (2004).
- [44] D. V. Patil and K. N. Lakshmisha, *J. Comput. Phys.* **228**, 5262 (2009).
- [45] X. W. Shan and H. D. Chen, *Phys. Rev. E* **47**, 1815 (1993).
- [46] M. R. Swift, W. R. Osborn, and J. M. Yeomans, *Phys. Rev. Lett.* **75**, 830 (1995).
- [47] A. Lamura, G. Gonnella, and J. M. Yeomans, *Europhys. Lett.* **45**, 314 (1999).

- [48] T. Inamuro, T. Ogata, S. Tajima, and N. Konishi, *J. Comput. Phys.* **198**, 628 (2004).
- [49] T. H. Lee and C. L. Lin, *J. Comput. Phys.* **206**, 16 (2005).
- [50] J. M. Yeomans, *Physica A* **369**, 159 (2006).
- [51] M. Sbragaglia, R. Benzi, L. Biferale, S. Succi, and F. Toschi, *Phys. Rev. Lett.* **97**, 204503 (2006).
- [52] T. Inamuro, *Fluid. Dyn. Res.* **38**, 641 (2006).
- [53] A. Xu, G. Gonnella, and A. Lamura, *Phys. Rev. E* **74**, 011505 (2006).
- [54] S. Arcidiacono, I. V. Karlin, J. Mantzaras, and C. E. Frouzakis, *Phys. Rev. E* **76**, 046703 (2007).
- [55] G. Gonnella, A. Lamura, and V. Sofonea, *Phys. Rev. E* **76**, 036703 (2007).
- [56] R. S. Saksena and P. V. Coveney, *J. Phys. Chem. B* **112**, 2950 (2008).
- [57] A. Tiribocchi, N. Stella, G. Gonnella, and A. Lamura, *Phys. Rev. E* **80**, 026701 (2009).
- [58] C. K. Aidun and J. R. Clausen, *Annu. Rev. Fluid. Mech.* **42**, 439 (2010).
- [59] M. Sbragaglia, R. Benzi, L. Biferale, H. Chen, X. Shan, and S. Succi, *J. Fluid Mech.* **628**, 299 (2009).
- [60] A. Cristea, G. Gonnella, A. Lamura, and V. Sofonea, *Commun. Comput. Phys.* **7**, 350 (2010).
- [61] S. Ansumali and I. V. Karlin, *Phys. Rev. E* **66**, 026311 (2002).
- [62] F. Toschi and S. Succi, *Europhys. Lett.* **69**, 549 (2005).
- [63] M. Sbragaglia and S. Succi, *Phys. Fluids* **17**, 093602 (2005).
- [64] R. Benzi, L. Biferale, M. Sbragaglia, S. Succi, and F. Toschi, *J. Fluid Mech.* **548**, 257 (2006).
- [65] M. Sbragaglia and S. Succi, *Europhys. Lett.* **73**, 370 (2006).
- [66] I. V. Karlin and S. Ansumali, *Phys. Rev. E* **76**, 025701(R) (2007).
- [67] S. Ansumali, I. V. Karlin, S. Arcidiacono, A. Abbas, and N. I. Prasianakis, *Phys. Rev. Lett.* **98**, 124502 (2007).
- [68] W. P. Yudistiawan, S. Ansumali, and I. V. Karlin, *Phys. Rev. E* **78**, 016705 (2008).
- [69] S. H. Kim, H. Pitsch, and I. D. Boyd, *Phys. Rev. E* **77**, 026704 (2008).
- [70] S. H. Kim and H. Pitsch, *Phys. Rev. E* **78**, 016702 (2008).
- [71] S. H. Kim, H. Pitsch, and I. D. Boyd, *J. Comput. Phys.* **227**, 8655 (2008).
- [72] G. H. Tang, Y. H. Zhang, and D. R. Emerson, *Phys. Rev. E* **77**, 046701 (2008).
- [73] D. Lockerby and J. M. Reese, *J. Fluid Mech.* **604**, 235 (2008).
- [74] S. S. Chikatamarla and I. V. Karlin, *Phys. Rev. E* **79**, 046701 (2009).
- [75] W. P. Yudistiawan, S. K. Kwak, D. V. Patil, and S. Ansumali, *Phys. Rev. E* **82**, 046701 (2010).
- [76] X. J. Gu and D. R. Emerson, *J. Fluid Mech.* **636**, 177 (2009).
- [77] J. M. Reese and Y. H. Zhang, *J. Comput. Theor. Nanoscience* **6**, 2061 (2009).
- [78] Y. Sone, *Kinetic Theory and Fluid Dynamics* (Birkhäuser, Boston, 2002).
- [79] G. Karniadakis, A. Beskok, and N. Aluru, *Microflows and Nanoflows: Fundamentals and Simulation* (Springer, Berlin, 2005).
- [80] H. Struchtrup, *Macroscopic Transport Equations for Rarefied Gas Flows* (Springer, Berlin, 2005).
- [81] C. Shen, *Rarefied Gas Dynamics: Fundamentals, Simulations and Micro Flows* (Springer, Berlin, 2005).
- [82] *MEMS Handbook, Volume I: Introduction and Fundamentals*, edited by M. Gad-el-Haq, (CRC Press, Boca Raton, FL, 2006).
- [83] Y. Sone, *Molecular Gas Dynamics: Theory, Techniques and Applications* (Birkhäuser, Boston, 2007).
- [84] L. Mieussens and H. Struchtrup, *Phys. Fluids* **16**, 2797 (2004).
- [85] H. Struchtrup and M. Torrilhon, *Phys. Rev. Lett.* **99**, 014502 (2007).
- [86] M. Torrilhon and H. Struchtrup, *J. Comput. Phys.* **227**, 1982 (2008).
- [87] H. Struchtrup and M. Torrilhon, *Phys. Rev. E* **78**, 046301 (2008).
- [88] P. Taheri, M. Torrilhon, and H. Struchtrup, *Phys. Fluids* **21**, 017102 (2009).
- [89] X. W. Shan and X. Y. He, *Phys. Rev. Lett.* **80**, 65 (1998).
- [90] R. Y. Zhang, X. W. Shan, and H. D. Chen, *Phys. Rev. E* **74**, 046703 (2006).
- [91] H. D. Chen and X. W. Shan, *Physica D* **237**, 2003 (2008).
- [92] B. Piaud, S. Blanco, R. Fournier, and M. J. Clifton, *J. Stat. Phys.* **121**, 119 (2005).
- [93] B. Piaud, Ph.D. Thesis, University Paul Sabatier, Toulouse, 2007.
- [94] X. Y. He and L. S. Luo, *Phys. Rev. E* **56**, 6811 (1997).
- [95] J. W. Shim and R. Gatignol, *Phys. Rev. E* **83**, 046710 (2011).
- [96] E. M. Shakov, *Fluid Dyn.* **3**, 95 (1968).
- [97] E. M. Shakov, *Fluid Dyn.* **3**, 112 (1968).
- [98] V. A. Titarev, *Comput. Fluids* **36**, 1446 (2007).
- [99] I. A. Graur and A. P. Polikarpov, *Heat Mass Transfer* **46**, 237 (2009).
- [100] V. Sofonea and R. F. Sekerka, *Phys. Rev. E* **71**, 066709 (2005).
- [101] M. Watari, *Physica A* **382**, 502 (2007).
- [102] M. Watari, *Phys. Rev. E* **79**, 066706 (2009).
- [103] M. Watari, *J. Fluid Eng.* **132**, 101401 (2010).
- [104] I. P. Mysovskikh, *Soviet Math. Dokl.* **36**, 229 (1988).
- [105] D. Zwillinger, *Handbook of Integration* (Jones and Bartlett, Boston, 1992).
- [106] M. Abramowitz and I. A. Stegun, *Handbook of Mathematical Functions (10th printing)* (National Bureau of Standards, Washington, DC, 1972).
- [107] F. B. Hildebrand, *Introduction to Numerical Analysis (2nd ed.)* (Dover, New York, 1987).
- [108] V. G. Vincenti and C. H. Kruger, *Introduction to Physical Gas Dynamics* (Wiley, New York, 1982).
- [109] R. J. LeVeque, *Numerical Methods for Conservation Laws* (Birkhäuser, Basel, 1992).
- [110] E. F. Toro, *Riemann Solvers and Numerical Methods for Fluid Dynamics* (Springer, Berlin, 1999).
- [111] A. Cristea and V. Sofonea, *Cent. Eur. J. Phys.* **2**, 382 (2004).
- [112] V. Sofonea and R. F. Sekerka, *Int. J. Mod. Phys. C* **16**, 1075 (2005).
- [113] A. Cristea, G. Gonnella, A. Lamura, and V. Sofonea, *Math. Comput. Simul.* **72**, 113 (2006).
- [114] M. Botti, G. Gonnella, A. Lamura, F. Massaioli, and V. Sofonea, *Int. J. Mod. Phys. C* **19**, 1847 (2008).
- [115] G. Gonnella, A. Lamura, and V. Sofonea, *Eur. Phys. J. Special Topics* **171**, 181 (2009).
- [116] V. Sofonea, *J. Comput. Phys.* **228**, 6107 (2009).
- [117] V. Sofonea, *Phys. Rev. E* **74**, 056705 (2006).
- [118] V. Sofonea, *Europhys. Lett.* **76**, 829 (2006).
- [119] A. Schuetze, *Direct Simulation by Monte Carlo Modeling Couette Flow using dsmcIas.f: A user's manual*, Report, Department of Mechanical Engineering, University of Victoria, Canada, 2003 (unpublished).

- [120] Y. Shi, P. L. Brookes, Y. W. Yap, and J. E. Sader, *Phys. Rev. E* **83**, 045701 (2011).
- [121] L. de Izarra, J. L. Rouet, and B. Izrar, *Phys. Rev. E* **84**, 066705 (2011).
- [122] Y. Zheng and H. Struchtrup, *Phys. Fluids* **17**, 127103 (2005).
- [123] L. Mieussens, *J. Comput. Phys.* **162**, 429 (2000).
- [124] L. Mieussens, *Math. Models Meth. Appl. Sci.* **10**, 1121 (2000).
- [125] S. Balay, K. Buschelman, V. Eijkhout, W. Gropp, D. Kaushik, M. Knepley, L. Curfman McInnes, B. Smith, and H. Zhang, *PETSc Users Manual*, Technical Report No. ANL-95/11–Revision 3.1 (2010), Argonne National Laboratory, [<http://www.mcs.anl.gov/petsc>].
- [126] H. Grad, *Commun. Pure Appl. Maths* **2**, 325 (1949).